

**A Spherical Magnetic Dipole Actuator for Spacecraft
Attitude Control**

by

J. A. Chabot

B.S., University of New Hampshire, 2013

A thesis submitted to the
Faculty of the Graduate School of the
University of Colorado in partial fulfillment
of the requirements for the degree of
Master of Science
Department of Aerospace Engineering Sciences
2015

This thesis entitled:
A Spherical Magnetic Dipole Actuator for Spacecraft Attitude Control
written by J. A. Chabot
has been approved for the Department of Aerospace Engineering Sciences

Hanspeter Schaub

Brandon Jones

Jeffrey Parker

Date _____

The final copy of this thesis has been examined by the signatories, and we find that both the content and the form meet acceptable presentation standards of scholarly work in the above mentioned discipline.

Chabot, J. A. (M.S., Aerospace Engineering)

A Spherical Magnetic Dipole Actuator for Spacecraft Attitude Control

Thesis directed by Prof. Hanspeter Schaub

Spacecraft generally require multiple attitude control devices to achieve full attitude actuation because of the limited control authority a single, traditional device can provide. This work presents a new momentum-exchange device that has the potential to replace traditional attitude control systems with a single actuator, in turn providing mass, volume, and power savings. The proposed actuator consists of a spherical dipole magnet enclosed in an array of coils that are fixed to the spacecraft body. Excitation of the coils as prescribed by the control law accelerates the dipole magnet in such a manner as to produce a desired reaction torque for orienting the spacecraft. The coils also control the magnet's position inside the spacecraft body via a separate control law, which is necessary because of the non-contact nature of the device. Analytical force and torque models are developed and are used in single and dual actuator attitude control schemes. Simulations conducted so far indicate that full attitude control is possible from a single device despite the axisymmetric field of the magnetic dipole rotor, which was anticipated to cause underactuation issues. Additionally, a dual actuator system is investigated to provide control redundancy, which is desirable in many missions. Finally, the single actuator system is compared to a cluster of three reaction wheels, illustrating how this device can provide mass, volume, and power savings.

Dedication

To my parents, Guy and Sue, for all your love and support. I'll try to repay you after this research makes me rich.

Acknowledgements

There are too many people to name who have helped me along the path to this point, but I guess I'll try and name a few. First off, I want to thank my thesis advisor, Dr. Hanspeter Schaub, for his invaluable insight and guidance with this research – a ten minute talk with him can usually solve months' worth of woe. Going back to my time at the University of New Hampshire, my advisor Dr. May-Win Thein also played a huge role in this research; she inspired me to get into attitude dynamics and controls, which eventually led to this thesis. Both Dr. Thein and Schaub are spectacular advisors who are truly invested in their students. I also want to thank my friends in the Autonomous Vehicle Systems lab for the good times and for their moral support.

Aside from those in academia, I'd like to thank my parents for all they've done for me – none of this would have been possible if it weren't for them. I also want to thank my younger brother, Zack, who I know will always be there for me. Thanks to my friends, as well, for distracting me and keeping me sane – I'd probably be a crazy recluse by now if it weren't for them. Finally and most importantly, I'd like to thank my cat for keeping me company while writing this thesis.

Contents

Chapter	
1 Introduction	1
1.1 Traditional Attitude Control Systems	1
1.2 Motivation behind Spherical Attitude Actuators	4
1.2.1 Asynchronous Spherical Actuators	5
1.2.2 Synchronous Spherical Actuators	7
1.3 Spherical Magnetic Dipole Actuator	8
2 Mathematical Formulations	10
2.1 Equations of Motion for Spacecraft with Three Reaction Wheels	10
2.2 Equations of Motion for Spacecraft with n -Spherical Actuators	13
2.3 Spherical Actuator Model	14
2.4 Actuator Electrical Power Model	18
2.5 Spacecraft Attitude Control	19
3 Numerical Simulations	23
3.1 Validation of Centered Rotor Assumption	23
3.2 Off-Center Actuator Analysis	24
3.3 Single Actuator Attitude Control	26
3.4 Dual Actuator Attitude Control	29
3.5 Null Motion Singularity Avoidance	31

4	Comparison to Reaction Wheel System	33
5	Conclusions	36
	Bibliography	39
	Appendix	
A	Algebraic Force and Torque Expressions	46

Tables

Table

3.1	Simulation Parameters	23
4.1	ACS Parameter Comparison	34

Figures

Figure

1.1	A set of 3 reaction wheels.	2
1.2	Single-Axis Control Moment Gyro	3
1.3	Diagram of Haeusseraiann's Patent	4
1.4	Asynchronous Spherical Actuator	6
1.5	Synchronous Spherical Actuator	8
1.6	Spherical Dipole Actuator with 20 Coils	9
2.1	Reaction Wheel Coordinate Frame Illustration.	10
2.2	Definition of Spherical Actuator Coordinate Frames	15
2.3	Coil Coordinate Frame	16
2.4	Diagram illustrating magnetic moment vector angle ϕ	22
3.1	Comparison of Centered and Off-Centered Rotor	24
3.2	Comparison of actuator at different distances from center of mass.	25
3.3	Single Actuator Attitude Control Maneuver	27
3.4	Illustration of Time-Varying Field Controllability	28
3.5	Single Actuator Control Near Singularity	29
3.6	Dual Actuator Attitude Control Maneuver	30
3.7	Dual Actuator Attitude Control Maneuver	32
4.1	ACS Comparison	33

4.2 Reaction Wheel Cluster Attitude Control Maneuver 35

Chapter 1

Introduction

1.1 Traditional Attitude Control Systems

The attitude control system (ACS) is a crucial part of nearly all spacecraft, integral to many aspects of a mission, such as pointing the spacecraft's solar panels at the sun to charge the batteries, aiming antennae towards earth or other satellites for communication, or pointing science instruments, such as a telescope, at a desired location in the sky. And of course if the ACS fails, communication can be lost, the spacecraft can run out of power and die, or science can't be collected.

Thrusters can be used for attitude control, however they are generally reserved for larger maneuvers, such as changing or maintaining an orbit, or as a backup attitude control system should the main ACS fail. A popular type of attitude control actuator found on spacecraft are momentum-exchange devices – namely, reaction wheels (RWs) and control moment gyros (CMGs). These devices work by transferring angular momentum between the spacecraft body and spinning momentum storage wheels. This transfer of angular momentum in turn alters the spacecraft's body rates and attitude.

Reaction wheels are a common choice in spacecraft because they are relatively simple devices and do not have control singularities. At its core, a reaction wheel control system is composed of a set of momentum wheels whose spin axes are fixed to the spacecraft body. By accelerating the wheels, a reaction torque is applied to the spacecraft, altering its attitude. A minimum of three reaction wheels, whose spin axes span 3D space, is required on a spacecraft for full attitude control,

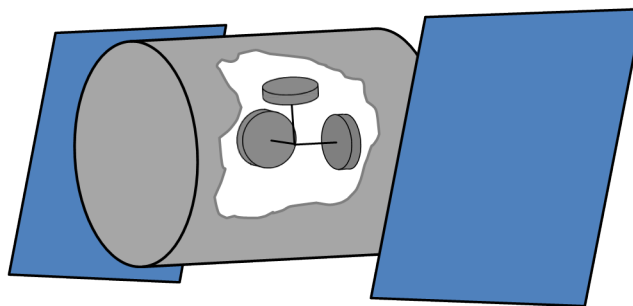


Figure 1.1: A set of 3 reaction wheels.

such as the cluster shown in Figure 1.1. However, four or more reaction wheels are often used for control redundancy in case of failure.

Although they are singularity free, one issue reaction wheels can encounter is wheel speed saturation. Over the course of a mission, the attitude control system must compensate for disturbance torques, such as atmospheric drag, to maintain a desired attitude. This can cause angular momentum to build-up in the reaction wheels leading them to eventually reach their momentum storage limit, which is directly related to wheel speed. As such, a spacecraft with reaction wheels will generally have a means for removing or “dumping” angular momentum, such as magnetorquers or thrusters. These devices provide external torques on a spacecraft system that can reduce the angular momentum stored in the reaction wheels, preventing them from saturating. Along with wheel saturation, a reaction wheel cluster with a large total angular momentum can make it difficult to reorient a spacecraft to a desired attitude.

Magnetorquers are coils of wire that interact with an external magnetic field, such as the Earth’s, when current is sent through them. They produce very little torque because of the strength of the external magnetic field, however magnetorquers have been used as the sole means for attitude control in some satellites and are discussed further in Section 3.3.

Unlike reaction wheels where the momentum storage component is fixed to the spacecraft body, a CMG consists of a spinning wheel that can be gimballed about one or two axes depending on the design. Figure 1.2 illustrates a single-axis CMG with a wheel spinning at a constant angular velocity of Ω and with a gimbal angle rate of $\dot{\gamma}$. In this instance, the gimbal axis is fixed to the

spacecraft body, allowing one degree of gimbal freedom. As such, a minimum of three CMGs is required for full attitude control. Gimbaling the momentum wheel amplifies the relatively small torque on the gimbal frame to a much larger torque on the spacecraft body. As such, CMGs require less energy than reaction wheels, in general, and are often used to control larger structures, such as the International Space Station where two dual-gimbal CMGs are used.

Drawbacks with CMGs include a relatively complex control strategy and a greater cost than RWs due to the complexity introduced by the gimbal mechanism. Additionally, CMGs can encounter singular gimbal angle configurations where the CMG cluster is unable to produce the desired torque or sometimes any torque at all. Control schemes have been developed to avoid these singularities and use techniques such as varying the wheel speed, Ω , effectively combining the benefits of a reaction wheel and a CMG. As mentioned, dual-axis CMGs exist where the gimbal frame can rotate with two degrees of freedom. They are less prone to singularity issues, however they are also more expensive than single-axis CMGs because of the increased mechanical complexity of the device [1].

A nice feature of CMGs, reaction wheels, and magnetorquers is they are all electrically powered, and so long as there is power aboard the spacecraft, these devices will work. This is a major reason why they are favored over thrusters, which rely on a finite amount of fuel.

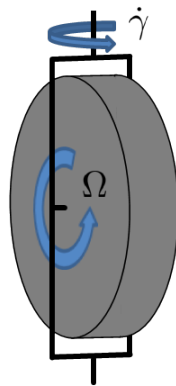


Figure 1.2: Single-Axis Control Moment Gyro

1.2 Motivation behind Spherical Attitude Actuators

The concept of a spherical attitude actuator is very similar to that of a reaction wheel – by accelerating a mass about an axis, a reaction torque is imparted on the spacecraft. With a spherical actuator however, that axis of rotation can be arbitrary. The first spherical actuator for attitude control was patented in 1960 by Haeusseraiann [2]. His design, shown in Figure 1.3, consists of a spherical mass suspended by an air bearing or magnetic field that can be accelerated about an arbitrary axis via jets of gas or a changing magnetic field.

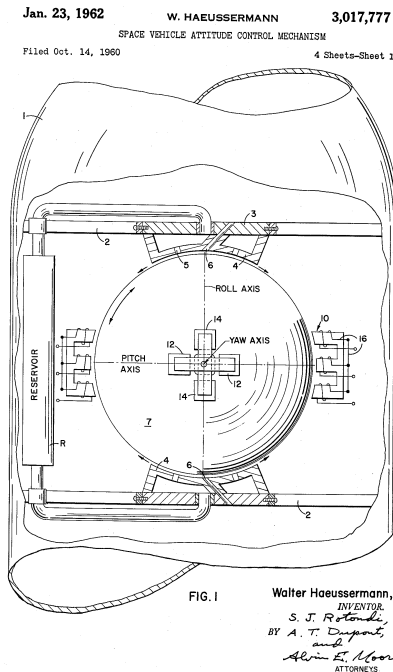


Figure 1.3: Diagram of Haeusseraiann’s patent for a spherical attitude actuator [2].

A similar patent published by Heinrich in 1961 cites the lack of gyroscopic effects, which are inherent in reaction wheels, as the impetus behind the pursuit of a spherical actuator because “evaluation of these effects can be accomplished only by a highly complicated electronic computer” [3]. Of course navigation processors aboard spacecraft today have no issue calculating these gyroscopic effects, leaving the promise of 3-DOF attitude control from a single device the driving force behind research in this area.

Having a single actuator provide full attitude control is very appealing because it has the potential to reduce ACS mass, volume, and power requirements, all of which greatly impact the cost of a mission. Spherical actuators also have the potential to reduce vibrational noise in a spacecraft and to increase the ACS lifespan. Both of these features stem from the non-contact nature of the spherical actuator. Conventional bearing systems are not well suited for spherical motion, and therefore the spherical mass must be suspended by other means. Additionally, mechanical contact in traditional bearing systems causes vibrations in a spacecraft, which are undesirable in missions where precision attitude pointing is necessary. Mechanical bearings are also often the source of ACS failure due to wear caused by physical contact.

In essence, spherical actuators are three-dimensional extensions of conventional electric motors, and as with conventional electric motors, spherical actuator designs fall under two general categories: synchronous and asynchronous. Asynchronous motors utilize a changing magnetic field to induce a current in a non-magnetic rotor. In turn, the induced current interacts with the changing magnetic field to produce a torque. Synchronous motors, on the other hand, rely on the interaction between permanent magnets and electromagnets. Coil excitation in the motor is timed via control logic to produce torque and spin the rotor. In general, asynchronous motors tend to be less efficient and have lower speed capabilities than synchronous motors, but are simpler and cheaper than synchronous motors [4].

1.2.1 Asynchronous Spherical Actuators

The majority of research into spherical actuators for attitude control conducted so far is focused on asynchronous-type designs. These designs fundamentally consist of a non-magnetic, conductive sphere, the rotor, that can be accelerated via a changing external magnetic field that is produced by an array of coils, the stator. Early designs such as those patented by Haeusseraiann and Heinrich propose using air bearings as a means of supporting the rotor [2, 3]. However, implementation of this on a spacecraft would be difficult as it requires an onboard, closed-loop, gas compression system to power the bearing.

Tierney and Ormsby later propose using electrostatic repulsion to suspend the rotor [5, 6]. Current designs, though, have moved away from using electrostatics due to the large electric potentials and hard vacuums needed and instead rely purely on induced effects for torque production and rotor suspension [7]. A large portion of the research in this area focuses on developing models, both analytical and numerical, for the induced currents in the rotor and for the force and torque production of the device [8–20]. Analytical solutions, however, are only available for simplified models due to the complicated magnetodynamics involved with the changing magnetic field.

Experimental investigations have been conducted to validate these models and move towards real world application [21–24]. Figure 1.4 shows Shirasawa’s experimental setup where a conductive rotor is suspended and torqued via a changing external field. In all of these asynchronous designs, eddy current losses pose a problem in terms of efficiency. Eddy currents are unfavorable, induced current flows inherently caused by the changing magnetic field. Conventional asynchronous motors have features in the rotor that guide the induced current, in turn reducing eddy currents and greatly improving efficiency. However because of the three-dimensional nature of this device, such eddy current mitigation features are difficult, if not impossible to include in the rotor design, therefore limiting the efficiency of the device. The induced currents will also cause heating of the rotor, which could be problematic because the rotor has no means of heat transfer aside from radiation across the vacuum gap between the rotor and stator.

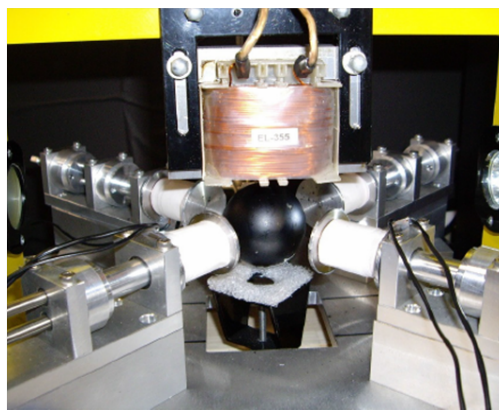


Figure 1.4: Asynchronous Spherical Actuator [24]

Along with research into asynchronous spherical actuators for attitude control, work has been done with robotics applications [25–27]. However, asynchronous actuators are often undesirable in these applications because they cannot provide the angular precision a synchronous motor can. As such, the majority of research into spherical actuators for robotics applications involves synchronous designs, which are covered in the next section.

1.2.2 Synchronous Spherical Actuators

In more recent years, synchronous spherical actuators for attitude control have gained interest thanks to the advancement of digital motor control electronics and the continually increasing computational power of microprocessors. In 1991, Nakanishi patented a “control moment gyro having [a] spherical rotor with permanent magnets” that consists of a rotor whose surface is embedded with a pattern of alternating magnetic poles [28]. In his invention, the stator coils control both the spin and gimbal angle of the rotor, leveraging the torque amplification properties of a CMG. To accomplish this, electronics control stator coil excitation in time with the motion of the permanent magnets in the rotor to produce torque and motion. This is similar to what occurs in permanent magnet DC motors and brushless DC motors.

Currently, Rossini et al. are the only group publishing research on synchronous actuators for attitude control. Their design consists of a rotor with eight equally distributed permanent magnets and a stator with 20 coils, as shown in Figure 1.5 [29, 30]. Analytical force and torque models for this actuator are developed and confirmed through finite-element modeling [31] and experimental investigations [32–34]. Also, their studies examine optimal stator sensor placement [31], rotor design optimization [35], back-EMF modeling [30], and eddy current losses [36, 37].

Although there is limited research into synchronous spherical actuators for attitude control, they have been studied in detail for robotics applications [38–68]. The spherical actuator is appealing from a robotics standpoint because it constitutes a fully actuated ball joint. The literature in this area examines various design aspects, such a magnetic pole placement [69], pole design [70, 71], coil placement [72], and coil modeling [73, 74]. For these robotics applications, there is generally a

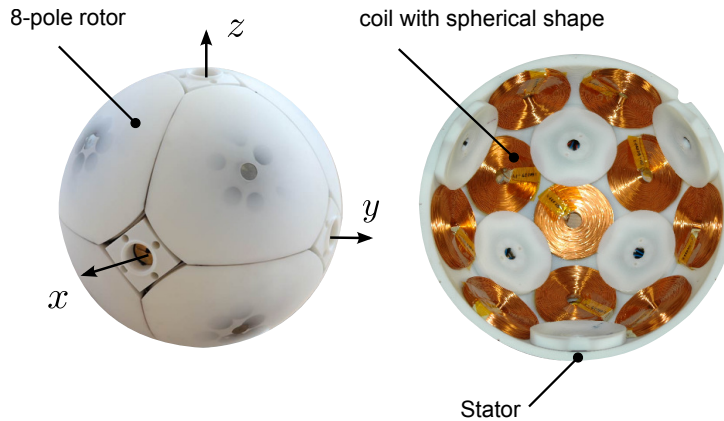


Figure 1.5: Synchronous Spherical Actuator [30]

means for torque transmission, such as a shaft, which limits the motion of the device. These devices also rely on a bearing system to support the rotor due to the presence of gravity and external loading depending on the application.

1.3 Spherical Magnetic Dipole Actuator

One difficulty with the synchronous designs proposed in the literature is the fabrication of the rotor, which is a collection of permanent magnets affixed to a substrate. For robotics applications where angular velocities are relatively low, the rotor does not need to be precisely balanced to be effective. However in momentum storage situations, such as with spacecraft attitude control, the rotor will reach very high spin rates and even small imbalances in the rotor will lead to large vibrations and potential destruction of the device. Because of this, the rotor would require precision machining of magnetic material, likely making the device difficult to manufacture and costly. Furthermore, the rotor structure must withstand the large centripetal forces that occur at high angular velocity.

The design proposed in this thesis instead uses a spherical dipole magnet as the rotor, as illustrated in Figure 1.6. Spherical dipole magnets are inexpensive, readily available, and produced from a homogeneous substrate, making them better-suited for high speed applications than multi-pole rotors. However, unlike with multi-pole rotors whose magnetic field is spherically symmetric,

a dipole rotor cannot provide an arbitrary torque at an instant in time because of the axisymmetry of its magnetic field. At first, this appears to be a major flaw in this design. However as will be seen in Section 3.3, control is actually possible from such a device. In the end, the spherical dipole actuator provides the mechanical simplicity of an asynchronous actuator with the efficiency of a synchronous actuator.

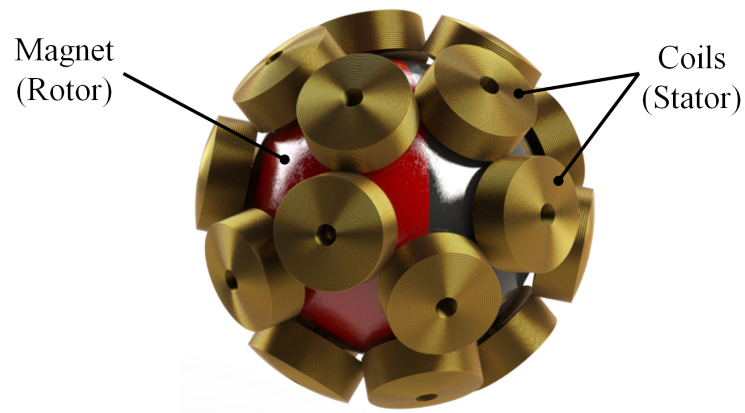


Figure 1.6: Spherical Dipole Actuator with 20 Coils

Chapter 2

Mathematical Formulations

2.1 Equations of Motion for Spacecraft with Three Reaction Wheels

A reaction wheel attitude control system is simulated in Chapter 4 for comparison against the proposed spherical actuator. As such, the equations of motion governing a spacecraft system with three reaction wheels aligned with the spacecraft principal axes of inertia are derived herein. Let us first define a spacecraft body-fixed frame, $\mathcal{B} : \{\hat{\mathbf{b}}_1, \hat{\mathbf{b}}_2, \hat{\mathbf{b}}_3\}$, where the coordinate axes are aligned with the principal axes of inertia of the spacecraft. Figure 4.1 illustrates the m^{th} reaction wheel in the cluster with its wheel-fixed coordinate frame defined as $\mathcal{W}_m : \{\hat{\mathbf{w}}_{s_m}, \hat{\mathbf{w}}_{a_m}, \hat{\mathbf{w}}_{b_m}\}$, where $\hat{\mathbf{w}}_{s_m} = \hat{\mathbf{b}}_m$. Note that all vector quantities are assumed to be given in the \mathcal{B} frame unless otherwise indicated.

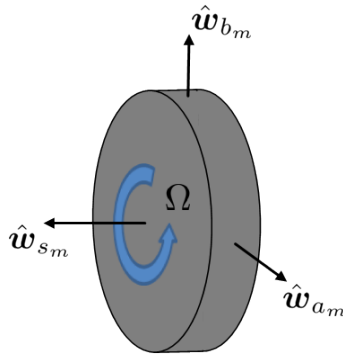


Figure 2.1: Reaction Wheel Coordinate Frame Illustration.

With this coordinate frame definition, the inertia tensor as seen from a wheel frame for a

given wheel is

$$\mathcal{W}_{[I_W]} = \begin{bmatrix} I_{W_s} & 0 & 0 \\ 0 & I_{W_t} & 0 \\ 0 & 0 & I_{W_t} \end{bmatrix} \quad (2.1)$$

where I_{W_s} is the inertia about the wheel spin axis and I_{W_t} is the wheel inertia about a transverse axis. All three wheels are assumed to have the same inertia properties in this derivation. The total angular momentum for the system is

$$\mathbf{H} = \mathbf{H}_B + \sum_{m=1}^3 \mathbf{H}_m \quad (2.2)$$

where \mathbf{H}_B is the angular momentum of the spacecraft body plus the transverse components of the wheel angular momenta and \mathbf{H}_m are the wheel angular momenta about their spin axes. The transverse components of wheel angular momenta are grouped with the first term in Eq. (2.2) because they are constant as seen from the spacecraft body frame, resulting in

$$\begin{aligned} \mathbf{H}_B &= [I_B] \boldsymbol{\omega}_{\mathcal{B}/\mathcal{N}} + I_{W_t} \sum_{m=1}^3 (\hat{\mathbf{w}}_{a_m} \hat{\mathbf{w}}_{a_m}^T + \hat{\mathbf{w}}_{b_m} \hat{\mathbf{w}}_{b_m}^T) \boldsymbol{\omega}_{\mathcal{B}/\mathcal{N}} \\ &= [I_B] \boldsymbol{\omega}_{\mathcal{B}/\mathcal{N}} + 2I_{W_t} \boldsymbol{\omega}_{\mathcal{B}/\mathcal{N}} \end{aligned} \quad (2.3)$$

where $[I_B]$ is the spacecraft body inertia tensor and $\boldsymbol{\omega}_{\mathcal{B}/\mathcal{N}}$ is the angular velocity of the spacecraft body with respect to some inertial frame \mathcal{N} . The angular momenta of the wheels about their spin axes, on the other hand, depend on wheel speeds. Therefore,

$$\begin{aligned} \sum_{m=1}^3 \mathbf{H}_m &= \sum_{m=1}^3 I_{W_s} (\omega_m + \Omega_m) \hat{\mathbf{w}}_{s_m} \\ &= I_{W_s} (\boldsymbol{\omega}_{\mathcal{B}/\mathcal{N}} + \boldsymbol{\Omega}) \end{aligned} \quad (2.4)$$

where Ω_m is the m^{th} wheel speed with respect to the spacecraft body and $\boldsymbol{\Omega}$ is the wheel speed vector. Eq. (2.2) can now be rewritten as

$$\mathbf{H} = ([I_B] + 2I_{W_t}[I_{3 \times 3}]) \boldsymbol{\omega}_{\mathcal{B}/\mathcal{N}} + I_{W_s} (\boldsymbol{\omega}_{\mathcal{B}/\mathcal{N}} + \boldsymbol{\Omega}) \quad (2.5)$$

The time rate of change of angular momentum about a system's center of mass is equivalent to the net external torque on the system:

$$\dot{\mathbf{H}} = \mathbf{L} \quad (2.6)$$

Because Eq. (2.5) is described in the \mathcal{B} frame, the transport theorem must be applied when taking the inertial derivative in Eq. (2.6):

$$\frac{\mathcal{N}d}{dt}(\mathbf{H}) = \frac{\mathcal{B}d}{dt}(\mathbf{H}) + \boldsymbol{\omega}_{\mathcal{B}/\mathcal{N}} \times \mathbf{H} = \mathbf{L} \quad (2.7)$$

resulting in

$$([I_B] + 2I_{W_t}[I_{3 \times 3}])\dot{\boldsymbol{\omega}}_{\mathcal{B}/\mathcal{N}} + \boldsymbol{\omega}_{\mathcal{B}/\mathcal{N}} \times [I_B]\boldsymbol{\omega}_{\mathcal{B}/\mathcal{N}} + I_{W_s}(\dot{\boldsymbol{\omega}}_{\mathcal{B}/\mathcal{N}} + \dot{\boldsymbol{\Omega}}) + \boldsymbol{\omega}_{\mathcal{B}/\mathcal{N}} \times I_{W_s}\boldsymbol{\Omega} = \mathbf{L} \quad (2.8)$$

Next, Eq. (2.6) can be applied to the individual wheel spin axis angular momenta:

$$\dot{\mathbf{H}}_m = I_{W_s}(\dot{\omega}_m + \dot{\Omega}_m)\hat{\mathbf{w}}_m + \boldsymbol{\omega}_{\mathcal{B}/\mathcal{N}} \times I_{W_s}(\omega_m + \Omega_m)\hat{\mathbf{w}}_m = \mathbf{L}_m \quad (2.9)$$

where \mathbf{L}_m is the external torque on the given wheel. At this point, it's beneficial to isolate the component of torque that causes the wheel acceleration, $\dot{\Omega}_m$, because this will provide a relationship between the reaction wheel motor input torque and the resulting torque on the spacecraft body. By the wheel coordinate frame definition, the first component of \mathbf{L}_m is the motor torque and will be denoted as u_m . Extracting the first component from Eq. (2.9) yields

$$u_m = I_{W_s}(\dot{\omega}_m + \dot{\Omega}_m) \quad (2.10)$$

which can be used to create a vector equation relating reaction wheel cluster torque to angular accelerations:

$$\boldsymbol{\tau} = I_{W_s}(\dot{\boldsymbol{\omega}} + \dot{\boldsymbol{\Omega}}) \quad (2.11)$$

where $\boldsymbol{\tau} = [u_1 \ u_2 \ u_3]^T$ is the vector of reaction wheel motor torques. Finally, Eq. (2.11) can be substituted into Eq. (2.8) producing

$$([I_B] + 2I_{W_t}[I_{3 \times 3}])\dot{\boldsymbol{\omega}}_{\mathcal{B}/\mathcal{N}} + \boldsymbol{\omega}_{\mathcal{B}/\mathcal{N}} \times [I_B]\boldsymbol{\omega}_{\mathcal{B}/\mathcal{N}} + \boldsymbol{\omega}_{\mathcal{B}/\mathcal{N}} \times I_{W_s}\boldsymbol{\Omega} + \mathbf{u} = \mathbf{L} \quad (2.12)$$

For the simulations presented in Chapter (4), there are no external torques on the spacecraft system and the wheel inertia is much smaller than that of the spacecraft body. Therefore, $[I_B] \gg 2I_{W_t}[I_{3 \times 3}]$ and Eq. (2.12) may be simplified to

$$[I_B]\dot{\boldsymbol{\omega}}_{\mathcal{B}/\mathcal{N}} = -\boldsymbol{\omega}_{\mathcal{B}/\mathcal{N}} \times [I_B]\boldsymbol{\omega}_{\mathcal{B}/\mathcal{N}} - \boldsymbol{\omega}_{\mathcal{B}/\mathcal{N}} \times I_{W_s}\boldsymbol{\Omega} - \mathbf{u} \quad (2.13)$$

2.2 Equations of Motion for Spacecraft with n -Spherical Actuators

The total angular momentum for a spacecraft with n -spherical actuators is simply the sum of the angular momenta of the spacecraft body and the n -spherical actuator rotors,

$$\mathbf{H} = \mathbf{H}_B + \sum_{m=1}^n \mathbf{H}_m \quad (2.14)$$

where \mathbf{H}_B is the spacecraft body angular momentum and \mathbf{H}_m are the spherical actuator momenta. Again, the time rate of change of angular momentum about the system's center of mass is equivalent to the net external torque on the system. Therefore, Eq. (2.6) may be applied

$$\dot{\mathbf{H}} = \dot{\mathbf{H}}_B + \sum_{m=1}^n \dot{\mathbf{H}}_m = \mathbf{L} \quad (2.15)$$

and additionally, each spherical actuator can be treated as a separate system whose angular momentum rate is caused by an external torque:

$$\dot{\mathbf{H}}_m = -\mathbf{u}_m \quad (2.16)$$

Note that the actuator torque \mathbf{u}_m is negative in this instance because, as will be seen in Section 2.3, the actuator torque model describes the torque on the actuator coils, whereas here torque on the rotor is of interest. Hence the need for the sign change. Eq. (2.16) can then be substituted into Eq. (2.15) producing

$$\dot{\mathbf{H}}_B - \sum_{m=1}^n \mathbf{u}_m = \mathbf{L} \quad (2.17)$$

Because \mathbf{H}_B is described in the spacecraft body frame, the transport theorem must be applied to take the inertial derivative:

$$\frac{\mathcal{B}d}{dt}(\mathbf{H}_B) + \boldsymbol{\omega}_{\mathcal{B}/\mathcal{N}} \times \mathbf{H}_B - \sum_{m=1}^n \mathbf{u}_m = \mathbf{L} \quad (2.18)$$

From the definition of angular momentum about a rigid body's center of mass and due to the fact that the spacecraft inertia tensor is constant as seen from the spacecraft body frame, Eq. (2.18) may then be rewritten as

$$[I_B] \dot{\boldsymbol{\omega}}_{\mathcal{B}/\mathcal{N}} + \boldsymbol{\omega}_{\mathcal{B}/\mathcal{N}} \times [I_B] \boldsymbol{\omega}_{\mathcal{B}/\mathcal{N}} = \sum_{m=1}^n \mathbf{u}_m + \mathbf{L} \quad (2.19)$$

where $\boldsymbol{\omega}_{\mathcal{B}/\mathcal{N}}$ is the spacecraft body rate vector with respect to an inertial frame and $[I_B]$ is the spacecraft body inertia tensor. As can be seen from Eq. (2.19), the torque produced by spherical actuators can be viewed as an external torque on the spacecraft. Additionally, Eq. (2.16) can be used to derive the equations of motion for the spherical actuators. Since the inertia of a sphere is identical whether viewed in a body or inertial frame, Eq. (2.16) can be rewritten as

$$[I_S]_m \dot{\boldsymbol{\omega}}_{\mathcal{R}_m/\mathcal{N}} = -\mathbf{u}_m \quad (2.20)$$

where $[I_S]_m$ denotes the m^{th} spherical actuator inertia and $\dot{\boldsymbol{\omega}}_{\mathcal{R}_m/\mathcal{N}}$ the m^{th} angular velocity with respect to an inertial frame.

2.3 Spherical Actuator Model

The development of the force and torque model for the proposed spherical actuator begins by examining the interaction between the rotor and an individual coil. Multiple coordinate frames are defined, as shown in Figure 2.2, where \mathcal{B} is a spacecraft body-fixed frame, \mathcal{R} is a frame fixed to the dipole rotor and aligned with its axis of magnetization, and \mathcal{C}_k is the k^{th} coil-fixed frame aligned with the axis of the k^{th} coil.

To find the force and torque on an individual coil caused by the magnetic field of the rotor, the Lorentz force law is first simplified by assuming there are no external electric fields present in the system:

$$d\mathbf{F}_k = (\rho \mathbf{E} + \mathbf{J} \times \mathbf{B}) dV = (\mathbf{J} \times \mathbf{B}) dV \quad (2.21)$$

where $d\mathbf{F}_k$ is the differential force on the coil current density \mathbf{J} caused by the external magnetic field \mathbf{B} . Eq. (2.21) is modified into a torque expression by taking the cross product between the

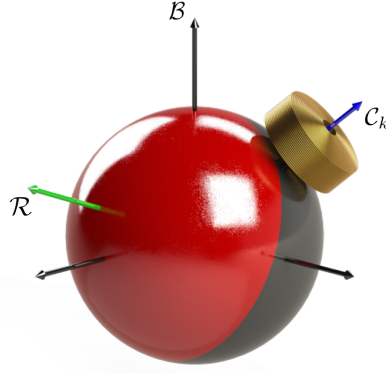


Figure 2.2: Definition of Spherical Actuator Coordinate Frames

position vector and the differential force element:

$$d\mathbf{T}_k = \mathbf{R} \times d\mathbf{F}_k = \mathbf{r} \times (\mathbf{J} \times \mathbf{B}) dV \quad (2.22)$$

Next, integrating Eqs. (2.21) and (2.22) over the volume of the coil yields the total force and torque acting on the coil:

$$\mathbf{F}_k = \int_V \mathbf{J} \times \mathbf{B} dV \quad (2.23a)$$

$$\mathbf{T}_k = \int_V \mathbf{R} \times \mathbf{J} \times \mathbf{B} dV \quad (2.23b)$$

These volume integrals can then be expanded into a useful form using spherical components, producing

$$\mathbf{F}_k = \int_{R_a}^{R_b} \int_{\theta_a}^{\theta_b} \int_{-\pi}^{\pi} \mathbf{J} \times \mathbf{B} R^2 \sin \theta d\phi d\theta dr \quad (2.24a)$$

$$\mathbf{T}_k = \int_{R_a}^{R_b} \int_{\theta_a}^{\theta_b} \int_{-\pi}^{\pi} \mathbf{R} \times \mathbf{J} \times \mathbf{B} R^2 \sin \theta d\phi d\theta dR \quad (2.24b)$$

As shown in Figure 2.3, parameterization with spherical components is convenient since the coil is a section of a sphere delimited by its inner and outer radii, R_a and R_b , its minor and major central angles, θ_a and θ_b , and its angle of revolution, ϕ . At this point in the development, it's useful to assign coordinate frames to the vectors. Because force and torque on a single coil are

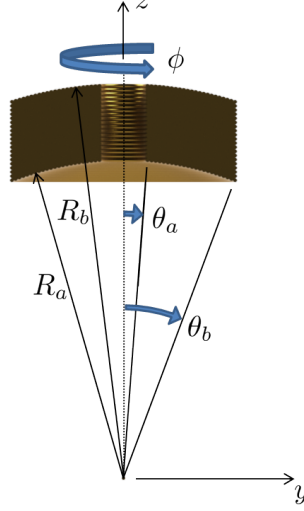


Figure 2.3: Coil Coordinate Frame

being examined, it is beneficial to express Eq. (2.24) in a local coil frame:

$$c_k \mathbf{F}_k = \int_{R_a}^{R_b} \int_{\theta_a}^{\theta_b} \int_{-\pi}^{\pi} c_k \mathbf{J} \times c_k \mathbf{B} R^2 \sin \theta \, d\phi \, d\theta \, dr \quad (2.25a)$$

$$c_k \mathbf{T}_k = \int_{R_a}^{R_b} \int_{\theta_a}^{\theta_b} \int_{-\pi}^{\pi} c_k \mathbf{R} \times c_k \mathbf{J} \times c_k \mathbf{B} R^2 \sin \theta \, d\phi \, d\theta \, dR \quad (2.25b)$$

where the position vector to a differential element in the coil frame is

$$c_k \mathbf{R} = \begin{pmatrix} R \sin \theta \cos \phi \\ R \sin \theta \sin \phi \\ R \cos \theta \end{pmatrix}, \quad (2.26)$$

and the current density vector is

$$c_k \mathbf{J} = \frac{i_k N}{A} \begin{pmatrix} -\sin \phi \\ \cos \phi \\ 0 \end{pmatrix} = \frac{2i_k N}{(R_b^2 - R_a^2)(\theta_b - \theta_a)} \begin{pmatrix} -\sin \phi \\ \cos \phi \\ 0 \end{pmatrix}. \quad (2.27)$$

In Eq. (2.27), i_k denotes the k^{th} coil current, N the number of turns in the coil, and A the cross-sectional area of the coil. Additionally, the magnetic field of the dipole rotor is given by

$$c_k \mathbf{B} = \frac{\mu_0}{4\pi} \left(\frac{3 c_k \boldsymbol{\rho} (c_k \mathbf{m} \cdot c_k \boldsymbol{\rho})}{\rho^5} - \frac{c_k \mathbf{m}}{\rho^3} \right) \quad (2.28)$$

where $\boldsymbol{\rho}$ is the relative position between a differential coil element and the center of the rotor:

$${}^{C_k}\boldsymbol{\rho} = {}^{C_k}\mathbf{R} - {}^{C_k}\mathbf{r} = {}^{C_k}\mathbf{R} - [{}^{C_k}\mathcal{B}]{}^{\mathcal{B}}\mathbf{r} \quad (2.29)$$

Here \mathbf{r} is the position of the rotor with respect to the center of the stator and $[{}^{C_k}\mathcal{B}]$ is the rotation matrix that transforms the rotor position from the body frame to the local coil frame. Also to express the rotor's magnetic field in the coil frame, the rotor's magnetic moment vector \mathbf{m} must be transformed:

$${}^{C_k}\mathbf{m} = [{}^{C_k}\mathcal{R}]{}^{\mathcal{R}}\mathbf{m} \quad (2.30)$$

Note that the third axis of the rotor frame is aligned with the rotor's axis of magnetization. With everything expressed in the common coil frame, the equations in (2.25) are integrated yielding the force and torque on a single coil. As it stands now, the integrals in Eq. (2.25) cannot be solved explicitly and must instead be integrated numerically. However, if the rotor is close to the center of the stator, $\mathbf{r} \ll \mathbf{R}$ and $\boldsymbol{\rho} \rightarrow \mathbf{R}$, and with this, analytical solutions to the volume integrals can be found. These algebraic expressions for \mathbf{F}_k and \mathbf{T}_k are provided in the Appendix for reference.

Finally, to get the overall force and torque produced by the spherical actuator given an arbitrary configuration of coils, the forces and torques from each of the coils must be described in the body frame and summed together:

$${}^{\mathcal{B}}\mathbf{f} = \sum_{k=1}^n [{}^{\mathcal{B}}\mathcal{C}_k] {}^{C_k}\mathbf{F}_k = [K_F] \mathbf{i} \quad (2.31a)$$

$${}^{\mathcal{B}}\boldsymbol{\tau} = \sum_{k=1}^n [{}^{\mathcal{B}}\mathcal{C}_k] {}^{C_k}\mathbf{T}_k = [K_T] \mathbf{i} \quad (2.31b)$$

where n is the number of coils in the system, $[{}^{\mathcal{B}}\mathcal{C}_k]$ transforms from the C_k frame to the \mathcal{B} frame, $[K_F]$ and $[K_T]$ are the $3 \times n$ force and torque characteristic matrices, and \mathbf{i} is the $n \times 1$ coil current vector [32]. If the rotor's position in the stator is accounted for in the derivations, then the characteristic matrices depend on the rotor's position and attitude and must be numerically integrated each time step. This numerical integration is prohibitively time-consuming for real-time application aboard a spacecraft. However, if the rotor is close enough to the center of the

stator, then the algebraic characteristic matrices provide a sufficient approximation and can be precomputed offline, allowing for real-time implementation.

2.4 Actuator Electrical Power Model

A useful measure of ACS performance is power consumption, which is related to the current draw of and electrical potential across the device. Here, the reaction wheel ACS will be modeled as a set of three DC motors, which have an established electrical model [4]. A common parameter used when discussing electric motors is the motor constant, K , which relates motor input current to output torque:

$$u = Ki \quad (2.32)$$

This motor torque relationship can be used in Eq. (2.13) to determine the necessary set of currents to affect the desired change in spacecraft state. Additionally, the voltage potential across a DC motor given a motor current i and motor speed ω is

$$V = iR + L \frac{d}{dt}(i) + V_{\text{emf}} \quad (2.33)$$

where R is the resistance across the motor, L is the inductance, and V_{emf} is the counter-electromotive force (or back-emf), which is caused by the changing magnetic field in the motor. These equations can then be used to find the motor power consumption via

$$P = iV \quad (2.34)$$

resulting in

$$P = Ri^2 + \frac{1}{2}L \frac{d}{dt}(i^2) + V_{\text{emf}}i \quad (2.35)$$

Equation (2.35) can be used to identify the components of power loss in a motor. The power dissipation due to thermal losses is given by

$$P_{\text{therm}} = Ri^2 \quad (2.36)$$

and the power stored in the changing magnetic field by

$$P_{\text{field}} = \frac{1}{2}L \frac{d}{dt}(i^2) \quad (2.37)$$

leaving the mechanical output power of the motor:

$$P_{\text{mech}} = V_{\text{emf}} i \quad (2.38)$$

By definition, rotational mechanical power in a system is given by

$$P_{\text{mech}} = u \omega = K i \omega \quad (2.39)$$

These two equations can be equated resulting in an expression for V_{emf} :

$$V_{\text{emf}} = K \omega \quad (2.40)$$

The preceding equations can then be expanded into vector form for application with the spherical actuator, as is described in Rossini [30], producing the following useful power equation:

$$P = \mathbf{V}^T \mathbf{i} = R \mathbf{i}^T \mathbf{i} + \frac{1}{2} \frac{d}{dt} (\mathbf{i}^T [L] \mathbf{i}) + \boldsymbol{\omega}_{\mathcal{B}/\mathcal{N}}^T [K_T] \mathbf{i} \quad (2.41)$$

Note that in this equation, the induction term $[L]$ is a matrix that describes the mutual and self induction of the coil array and that the motor constant $[K_T]$ is the matrix found in Eq. (2.31b). For the simulations presented in Chapters 3 and 4, the induction terms in Eq. (2.35) and Eq. (2.41) are assumed to be negligible compared to the other terms and are therefore neglected, as is common when creating a simplified motor model [4].

2.5 Spacecraft Attitude Control

Along with the spacecraft dynamics equations, an attitude parameterization is necessary. Modified Rodrigues Parameters (MRP) are chosen, and therefore the MRP attitude kinematic differential equation is given by

$$\dot{\boldsymbol{\sigma}} = \frac{1}{4} [(1 - \boldsymbol{\sigma}^T \boldsymbol{\sigma}) I_{3 \times 3} + 2\tilde{\boldsymbol{\sigma}} + 2\boldsymbol{\sigma} \boldsymbol{\sigma}^T] \boldsymbol{\omega} \quad (2.42)$$

where $\boldsymbol{\sigma}$ is the MRP attitude vector [1]. To avoid the MRP singularity, the norm of $\boldsymbol{\sigma}$ is kept less than or equal to unity by switching to the MRP shadow set when necessary. This also ensures that the shorter attitude control trajectory will be chosen.

The following feedback control law is used to stabilize the spacecraft relative to the attitude origin:

$$\boldsymbol{\tau} = \sum_{m=1}^n \mathbf{u}_m = -P\boldsymbol{\sigma} - [D]\boldsymbol{\omega} \quad (2.43)$$

where P is a positive scalar and $[D]$ is a positive-definite matrix. This attitude regulation control law is globally asymptotically stabilizing if no unmodeled torques are present, which is the case for all simulations presented here [1, 75]. Note that the following developments are not tied to this particular choice of attitude control law in Eq. (2.43). Rather, this proportional-derivative regulation control can be substituted with any desired attitude control torque expression, including a reference tracking control. Of interest is how this desired control torque $\boldsymbol{\tau}$ is generated through the rotors and coils.

The relationships between coil current and actuator force and torque that are established in Eq. (2.31) can now be used to calculate the necessary coil current vector given a desired spacecraft torque command. For the case where only a single spherical actuator is used,

$$\begin{bmatrix} K_T \\ K_F \end{bmatrix} \mathbf{i} = \begin{bmatrix} \boldsymbol{\tau} \\ \mathbf{f} \end{bmatrix} \quad (2.44)$$

relates coil currents to forces and torques. Here, the rotor position control force \mathbf{f} is given by a closed-loop feedback control law. A simple PD controller is chosen to provide rotor position control:

$$\mathbf{f} = -K_P \mathbf{r} - K_D \dot{\mathbf{r}} \quad (2.45)$$

where K_P and K_D are positive scalar gains, \mathbf{r} is the rotor position error, and $\dot{\mathbf{r}}$ is the rotor velocity error. The position error is given by

$$\mathbf{r} = \mathbf{D}' - \mathbf{D} \quad (2.46)$$

where \mathbf{D}' is the actual position of the rotor with respect to the spacecraft center of mass, which is time varying, and \mathbf{D} is the position of the center of the stator with respect to the center of mass, which is constant as seen from the body frame. Also, the velocity error is given by

$$\dot{\mathbf{r}} = \frac{\mathcal{B}_d}{dt}(\mathbf{D}') - \boldsymbol{\omega}_{\mathcal{B}/\mathcal{N}} \times \mathbf{D} \quad (2.47)$$

As will be seen in Chapter 3, the position of the rotor does not converge to zero unless the spherical actuator is at the center of mass of the spacecraft or if the spacecraft body rates are zero. This is because Eq. (2.45) is only a regulation control law. If the actuator is away from the center of mass and if the spacecraft has a body rate, a non-zero control effort will be needed to prevent the rotor from impacting the stator wall. The control law presented in Eq. (2.45) will only cause the rotor to converge to a steady-state, non-zero position trajectory. A reference tracking control law that feeds forward the dynamics of the spacecraft would likely control the rotor position to zero, though would still require a non-zero control effort because the controller is enforcing unnatural rotor dynamics.

The coil current vector in Eq. (2.44) can be found by applying a Moore-Penrose pseudoinverse:

$$\mathbf{i} = \begin{bmatrix} K_T \\ K_F \end{bmatrix}^+ \begin{bmatrix} \boldsymbol{\tau} \\ \mathbf{f} \end{bmatrix} \quad (2.48)$$

Because of the axisymmetry of the dipole rotor, $[K_T]$ is rank 2, and therefore there is a null space of torques that cannot be produced by the single actuator at an instant in time. In instances where a torque cannot be produced, the pseudoinverse finds the least-squares solution to the rank deficient problem. The characteristic force matrix $[K_T]$, however, is always full rank and can therefore provide the desired position control force. Although the rank deficiency of the torque matrix at first appears to cause issue, simulations and analogous underactuated systems indicate that full attitude control is still possible from a single device and is discussed in Chapter 3.

Although full control is likely possible from a single device, a second spherical actuator can be added to the system to remedy the rank deficiency and provide ACS redundancy, resulting in

$$\begin{bmatrix} K_{T1} & K_{T2} \\ K_{F1} & \mathbf{0} \\ \mathbf{0} & K_{F2} \end{bmatrix} \begin{pmatrix} \mathbf{i}_1 \\ \mathbf{i}_2 \end{pmatrix} = \begin{bmatrix} \boldsymbol{\tau} \\ \mathbf{f}_1 \\ \mathbf{f}_2 \end{bmatrix} \quad (2.49)$$

where the numeric subscripts indicate the first and second actuator. The pseudoinverse is again

needed to solve for the current vectors because the augmented matrix is rectangular,

$$\begin{pmatrix} \mathbf{i}_1 \\ \mathbf{i}_2 \end{pmatrix} = \begin{bmatrix} K_{T1} & K_{T2} \\ K_{F1} & \mathbf{0} \\ \mathbf{0} & K_{F2} \end{bmatrix}^+ \begin{bmatrix} \boldsymbol{\tau} \\ \mathbf{f}_1 \\ \mathbf{f}_2 \end{bmatrix}. \quad (2.50)$$

However, now the torque portion of Eq. (2.50) is rank 4, in general, and the system is overdetermined. The pseudoinverse therefore calculates the minimum current norm solution of the system. Despite this augmented configuration, there are instances where Eq. (2.50) becomes rank deficient. This occurs when the magnetic moment vectors of the two rotors are parallel, when $[K_{T1}] = [K_{T2}]$, as illustrated in Figure 2.4. In these instances, the system is equivalent to a single actuator. To

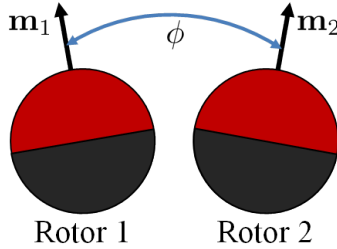


Figure 2.4: Diagram illustrating magnetic moment vector angle ϕ .

avoid alignment of the rotors, an equal magnitude and opposite sign torque can be applied to each of the rotors that drives them apart, while at the same time inducing no net torque on the spacecraft. This null motion torque is given by the following control law:

$$\mathbf{L}_n = \pm(K_1 \Delta\phi + K_2 \dot{\phi}) \left(\frac{\mathbf{m}_1 \times \mathbf{m}_2}{|\mathbf{m}_1 \times \mathbf{m}_2|} \right) \quad (2.51)$$

where K_1 and K_2 are positive scalar gains, \mathbf{m}_1 and \mathbf{m}_2 are the rotors' respective magnetic moment vectors, and $\Delta\phi$ is the error between the actual and desired angle between the magnetic moment vectors. This null motion torque can always be produced despite the torque matrix rank deficiency. This is because the null motion torque is perpendicular to the axis of symmetry of the rotor – the axis about which torque cannot be produced. Also, note that this null motion control law does not guarantee the rotors will not align. Should they, Eq. (2.51) encounters a singularity due to direction ambiguity of the null torque vector.

Chapter 3

Numerical Simulations

For all simulations in this chapter, the parameters in Table 3.1 are used. These design parameters were chosen such that the inertia about the rotor spin axis is equivalent to the spin axis inertia of the reaction wheel system discussed in Chapter 4. The rotor is also assumed to be solid and uniformly magnetized and to have no spin rate at the beginning of the maneuver. No initial spin rate was chosen for better comparison between different ACS configurations.

Table 3.1: Simulation Parameters

Parameter	Value	Parameter	Value
Number of Coils	20	Spacecraft Inertia, $[I]$	diag([0.02 0.03 0.08]) kg·m ²
Windings per Coil, N	334	Actuator 1 Position, D_1	[10 10 10] cm
Inner Coil Radius, R_a	20 mm	Actuator 2 Position, D_2	[-10 -10 -10] cm
Outer Coil Radius, R_b	24 mm	P Gain	0.008 N·m
Inner Coil Angle, θ_a	2.5°	$[D]$ Gain	[0.01 0.01 0.03] N·m·sec
Outer Coil Angle, θ_b	20°	K_P Gain	550 sec ⁻²
Rotor Radius	18 mm	K_D Gain	110 sec ⁻¹
Rotor Mass	182 g	Magnetic Moment, \mathbf{m}	25.66 N·m/T

3.1 Validation of Centered Rotor Assumption

As previously mentioned in Section 2.3, the volume integrals in Eq. (2.25) require numerical integration unless the rotor is centered within the stator. For real-time implementation, numerical volume integration is not an option due to its prohibitive computation time. However if the rotor is sufficiently centered in the stator, then the analytical solutions to the volume integrals are good

approximations. Since rotor position is controlled, the rotor remains close to the center and the analytical $[K_T]$ and $[K_F]$ matrices can be used.

Figure 3.1a shows the attitude error between a maneuver with an off-center rotor that needs numerical volume integration and the same maneuver with the rotor assumed perfectly centered in the stator, therefore using the analytical expressions. The attitude error between these two simulations of the same maneuver is measured in terms of the principal rotation angle. As can be seen, there are initial attitude differences due to the initial offset of the rotor, however the attitude differences are relatively small and converge to zero after the rotor becomes centered. This is also a worst-case scenario where the rotor is nearly touching the stator wall. Figure 3.1b displays how the rotor’s position in the stator converges to center thanks to the position control loop. The centered rotor approximation is therefore validated and is used in all subsequent simulations to drastically reduce simulation time. For comparison, the full model that uses numerical volume integration has a run-time of approximately 150 hours, whereas the analytical model only took 7 minutes.

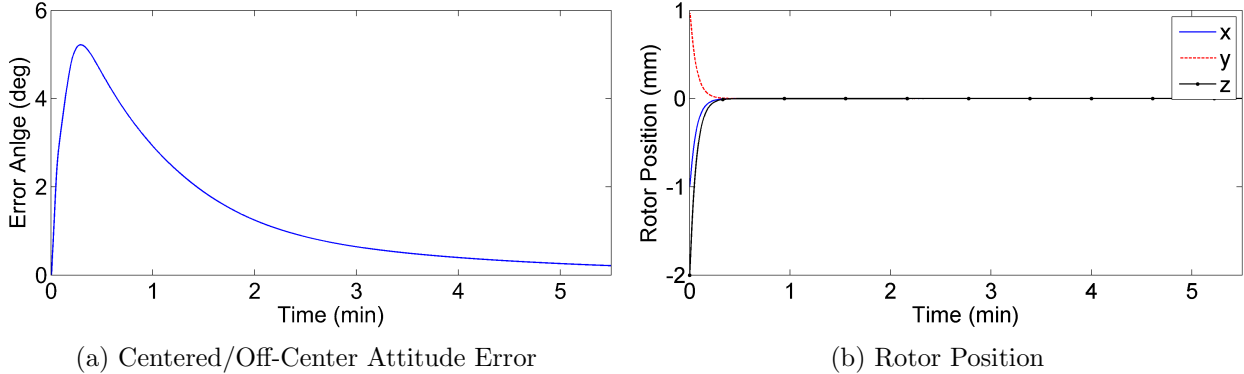


Figure 3.1: Comparison of Centered and Off-Centered Rotor

3.2 Off-Center Actuator Analysis

For most spacecraft, the ACS cannot be placed at the center of mass due to design requirements. This isn’t an issue with a reaction wheel system because the actuators can be put anywhere on the spacecraft so long as they span three dimensional space. However, the rotor position control

effort on a spherical actuator depends on its distance from the spacecraft center of mass and the spacecraft body rate, as indicated by the second term in Eq. 2.47.

Figure 3.2a shows the distance \mathbf{r} of the rotor from the center of the stator for two cases. The first case is a realistic situation where the spherical actuator is placed at $D_1 = [10 \ 10 \ 10]^T$ cm with respect to the spacecraft center of mass, and the spacecraft tumbles with an initial body rate of $\omega_{B/N} = [2 \ -1 \ 3]^T$ deg/sec. The second scenario is an extreme case where the actuator is placed at $D_1 = [200 \ 200 \ 200]^T$ cm (3.46 meters from the center) and the spacecraft is tumbling with $\omega_{B/N} = [40 \ -20 \ 60]^T$ deg/sec. In both cases the stator position does not converge to zero, which is expected because of the regulation position control law in place. With the first case where conditions are nominal, the offset from center is negligible and on the order of nanometers. However, the large stator center of mass distance and large body rates in the second case cause the rotor to deviate from center by between 0.28 mm to 0.63 mm. In this extreme case, the analytical model may not be a good enough approximation. Increasing the control gains will decrease the magnitude of the steady-state error, but will amplify noise in the system, which can lead to instability. A reference tracking control law would likely solve this steady-state trajectory issue and would drive rotor position to zero, permitting the use of a spherical actuator even in extreme situations.

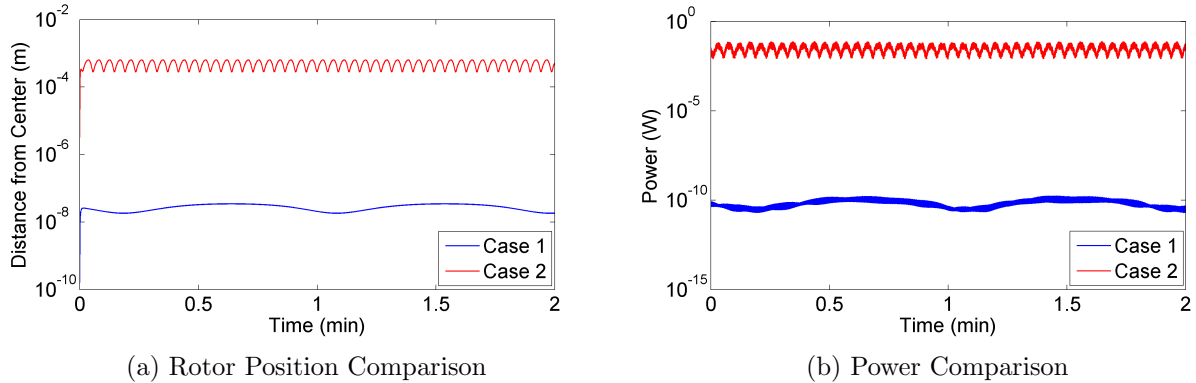


Figure 3.2: Comparison of actuator at different distances from center of mass.

Figure 3.2b illustrates the amount of power required to control the position of the rotor in the stator given the two scenarios. As can be seen from these power plots, even in extreme situations the

amount of position control power needed is very reasonable. For the nominal first case, the power consumption is negligible and on the order of nanowatts, and with the second extreme case, peak power consumption is 75 mW. Again, it's worth mentioning that the actuator power consumption does not converge to zero because the position controller is enforcing an unnatural rotor trajectory.

3.3 Single Actuator Attitude Control

The single actuator has proven to be effective at detumbling and pointing a spacecraft in numerical simulations conducted so far despite its inherent underactuation problem caused by the symmetry of the dipole field. Figures 3.3a and 3.3b illustrate this showing how the spacecraft attitude and body rate errors converge to zero. Additionally, the rotor's angular velocity converges to a steady-state value, as shown in Figure 3.3, which is due to the angular momentum originally contained in the spacecraft body that is completely transferred to the spinning rotor. The peak power consumption for the device occurs at the beginning of the maneuver and is 56.9 mW. The power consumption plot also illustrates how small the rotor position control effort is compared to the torque control effort. The total energy used by the actuator to perform this maneuver is 307 mJ.

Although it's not rigorously proven here, attitude controllability arguments can likely be made for the single actuator configuration. Only a subspace of control torques is available at an instant in time, however this subspace depends on the orientation of the rotor and is therefore time-varying. As long as there is enough variation in the orientation of the rotor, the control authority of the device will eventually span the torque space, resulting in controllability, despite the fact this is an underactuated device. In attitude control applications such as are presented here, the rotor's motion is periodic and will therefore have enough variation to span the torque space.

Attitude control of a spacecraft with three independent magnetorquers is a close analog to the spherical actuator and is controllable despite being underactuated, as is discussed in [76–81] and proven in [82]. With Earth's magnetic field modeled as a dipole, the torque capability of the three magnetorquers does not span three dimensional space at an instant in time, meaning the system

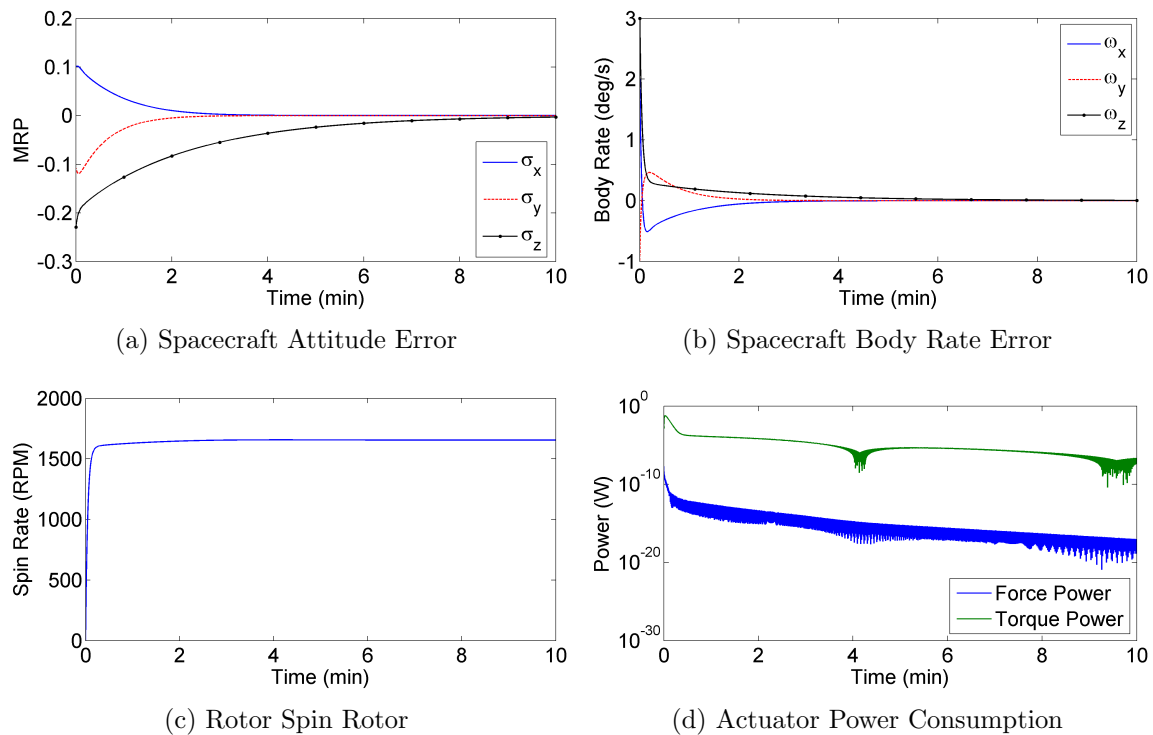


Figure 3.3: Single Actuator Attitude Control Maneuver

is underactuated. However, the controllable subspace of this system varies with the orbit of the spacecraft. As shown in the left-hand side of Figure 3.4, the magnetic field as seen by the spacecraft varies throughout the orbit. Over the period of an orbit, the three dimensional torque space that is necessary for full attitude control is covered because there is enough variation in the magnetic field, resulting in attitude controllability. With the spherical actuator, the dipole rotor is analogous to the Earth, and the array of coils analogous to the magnetorquers. The magnetorquers and coil array both span three dimensional space, however it's the axisymmetry of the dipole field that causes the instantaneous underactuation. As such, the controllability proof for the magnetically actuated spacecraft can likely be applied to the spherical actuator. As mentioned, simulation results thus far also point to this conclusion.

Both magnetic attitude control and the spherical actuator do suffer from a singularity, however. In the orbiting spacecraft attitude control scenario, controllability is lost if the spacecraft is in an equatorial orbit because there is no variation in the field as seen by the spacecraft. Similarly

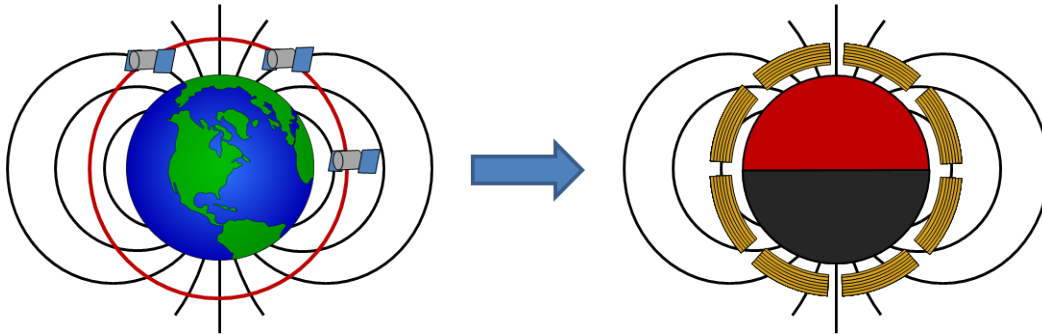


Figure 3.4: Illustration of Time-Varying Field Controllability

with the spherical actuator, a torque cannot be produced about the rotor magnetic moment vector. For instance, if a spin about the third spacecraft body axis is needed, but the rotor magnetic moment vector is perfectly aligned with the third body axis, then this spin cannot be accomplished. This scenario would not happen in reality, though, because this alignment of the magnetic moment vector would be instantaneous thanks to the relative motion between the spacecraft body and rotor. To illustrate this fact, Figure 3.5 is a worst-case scenario where the third spacecraft body axis and the rotor dipole axis are misaligned by 0.01° . Also, there is no initial relative motion between the spacecraft body and the rotor. Despite the fact the system is very close to a singular configuration, attitude control is still achieved. On top of this, control performance in terms of power consumption is not lost despite the proximity to the singularity, as is shown in Figure 3.5d, where peak power consumption is only 2.89 mW.

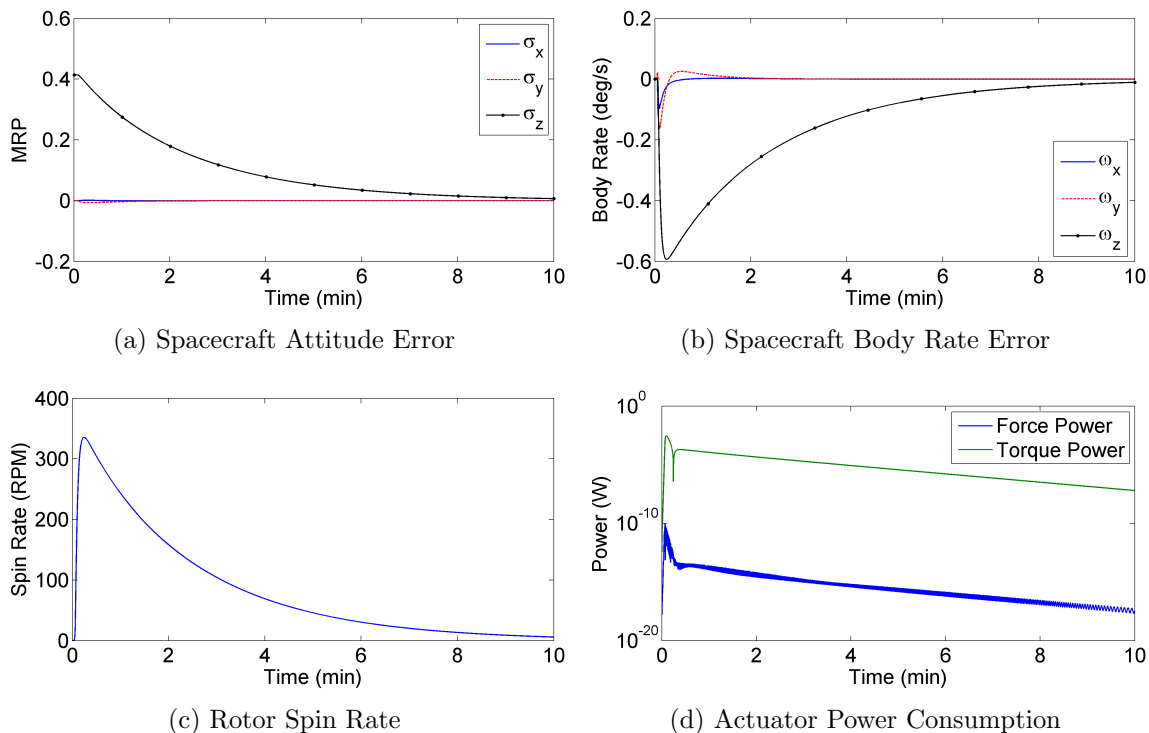


Figure 3.5: Single Actuator Control Near Singularity

3.4 Dual Actuator Attitude Control

Figure 3.6 displays the same attitude maneuver as was performed with the single actuator, only now with two spherical actuators, each with the same geometry and inertia as the single actuator. As can be seen, the performance is very similar to that which was provided by the single actuator. Interestingly, the dual actuator system has a lower peak power consumption of 30.5 mW at the beginning of the maneuver compared to the single actuator. The dual system also requires less energy, 221 mJ, to perform the maneuver than the single actuator, which is possibly due to the fact that the single actuator cannot produce an arbitrary torque at an instant in time. It could also be caused by the fact that the dual actuator system has twice as much momentum as the single actuator configuration.

One downside of the dual actuator system is that the rotors can end up in a spin configuration with high angular velocities despite relatively low or zero total system angular momentum.

This is because the angular momentum vectors of the rotors can point in opposite directions, in turn canceling each other out while still conserving the total angular momentum of the system. Controlling the final spin configuration of the rotors to eliminate unnecessary spin in the rotors is of interest and an area worth studying in future work.

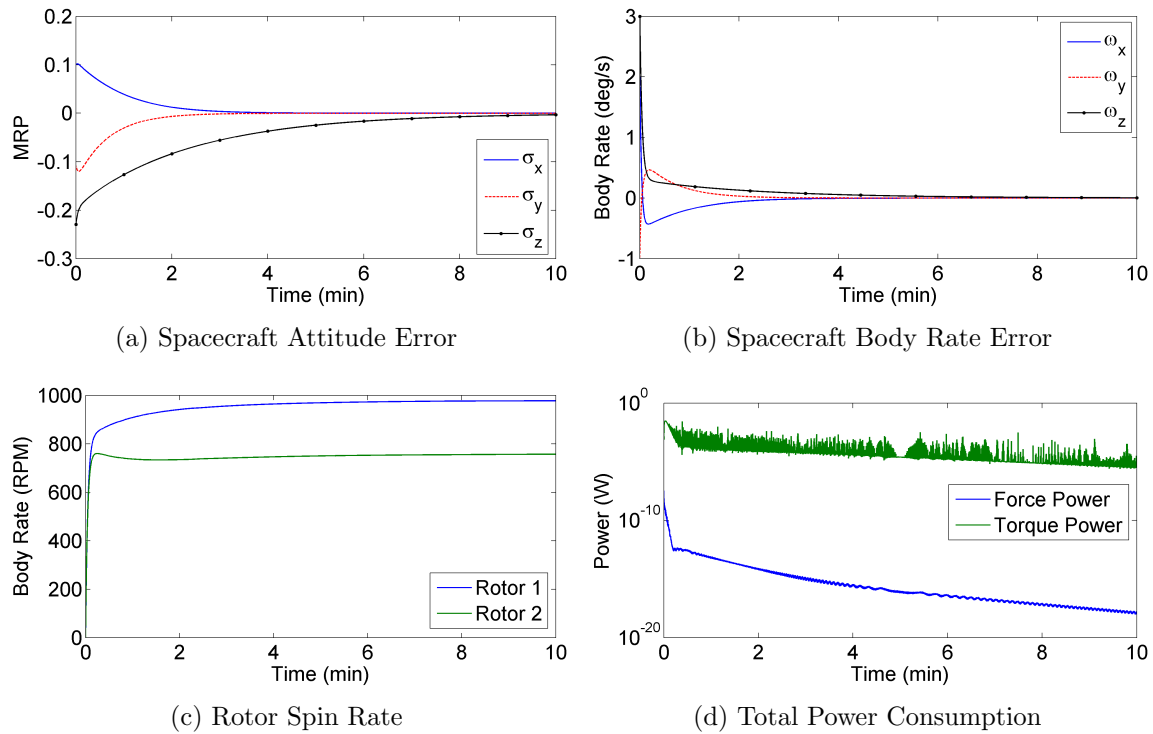


Figure 3.6: Dual Actuator Attitude Control Maneuver

3.5 Null Motion Singularity Avoidance

Equation (2.51) in Section 2.5 presented a control law to avoid alignment of the rotors in the dual actuator system. Again if the rotors align, the system degrades to an equivalent single spherical actuator, which Section 3.3 shows is not necessarily a bad thing. Regardless, the null motion control law is applied to the dual actuator system, and the results are presented in Figure 3.7. The control law gains were chosen to be $K_1 = 10^{-5} \text{ N} \cdot \text{m}$ and $K_2 = 10^{-5} \text{ N} \cdot \text{m} \cdot \text{sec}$ with a desired angle between rotors of $\phi = 90^\circ$.

Attitude control is achieved in this scenario, and additionally, the maneuver has a smaller peak power consumption than without the null motion control law. This is because the rotors in both dual actuator simulations are nearly aligned at the beginning of the simulation. The null motion control law drives the magnetic moment vectors apart, causing the rotors to better span three dimensional space, in turn requiring less power to produce the desired torque. For the simulation presented here, the null motion control law reconfigures the two rotors such that the magnetic moment vectors are perpendicular, and does so without imparting a torque on the spacecraft.

An interesting side effect of the null motion control law is that it causes the system to split the angular momentum stored in the two rotors equally, as shown in Figure 3.7c, where the rotors have equal spin magnitude throughout the maneuver, unlike what's seen in Figure 3.6c. As such, this null motion control could likely play a part in managing the final spin configuration of a dual actuator system. In the end however, the control effort needed to keep the rotors perpendicular to each other resulted in more energy needed to perform the maneuver than without the null motion control law – 1.05 J. Figure 3.7d shows how application of the null motion controller results in steady-state power consumption. This is caused by conservation of angular momentum in the system, which constrains the final spin configuration of the rotors, and because of this, the angle between the magnetic moment vectors cannot necessarily be controlled. Further research into singularity avoidance is needed to fully understand its benefits and limitations.

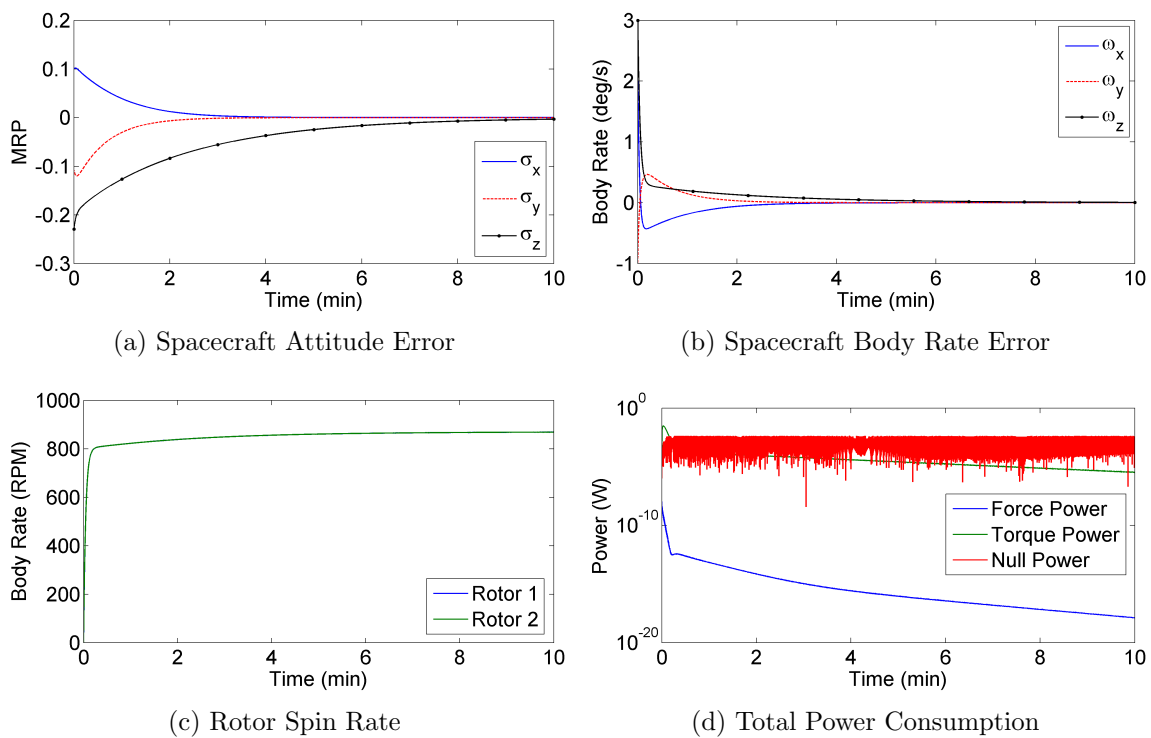


Figure 3.7: Dual Actuator Attitude Control Maneuver

Chapter 4

Comparison to Reaction Wheel System

Reaction wheel control systems are commonly found on spacecraft, and because of this, they serve as a good benchmark for judging the performance of the spherical actuator. The motor torque constant K is often used to compare motor capabilities, such as power consumption and efficiency. However with the spherical actuator, $[K_T]$ is time-varying making this difficult. As such, a reaction wheel ACS aboard a satellite is simulated to provide a comparison.

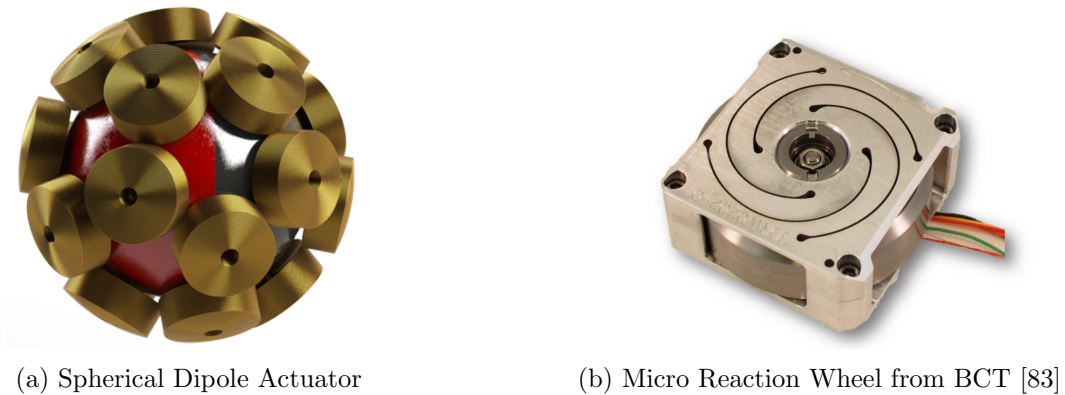


Figure 4.1: ACS Comparison

A commercially available reaction wheel system for small satellites sold by Blue Canyon Technologies (BCT) was chosen and is simulated using Eq. (2.13) and Eq. (2.35). An individual reaction wheel is shown beside the reaction sphere in Figure 4.1. The inertia, resistance, and motor constant used in this simulation were provided by BCT [83]. Figure 4.2 illustrates the same attitude maneuver used in Chapter 3, only now with a cluster of three reaction wheels. As expected, the

reaction wheel cluster has no issue controlling the spacecraft. Though not immediately apparent from the power plot, the reaction wheel system actually requires more power and energy than the single spherical actuator.

Table 4.1 provides a side-by-side comparison of some of the key parameters from these two simulations. The mass for the spherical actuator and reaction wheel cluster are similar, however the spherical actuator mass only accounts for the mass of the rotor and the coils. In an actual system, there would also be support structures and electronics that would add to the overall mass. The volumes for the two systems, however, are very different with the spherical actuator filling a volume almost half that of the reaction wheel cluster. Note that the spherical actuator volume is the spherical volume determined by the outer radius of the coils. Again, support structures and electronics are not included in this calculation and would likely increase the volume of the device. The reaction wheel cluster volume was determined by summing the individual volumes of the three reaction wheels as determined by the dimensions provided by BCT.

Table 4.1: ACS Parameter Comparison

	Spherical Actuator	Reaction Wheel Cluster
Inertia	240 g · cm ²	240 g · cm ²
Mass	311 g	345 g
Volume	57.9 cm ³	99.85 cm ³
Peak Power	56.9 mW	217 mW
Maneuver Energy	309 mJ	678 mJ

As mentioned earlier, the inertia about a spin axis for each device is matched to provide a basis for comparison. However, the reaction wheel cluster in this simulation can actually store more momentum than an individual axis because the total angular momentum of the cluster is the vector sum of the individual reaction wheel momenta.

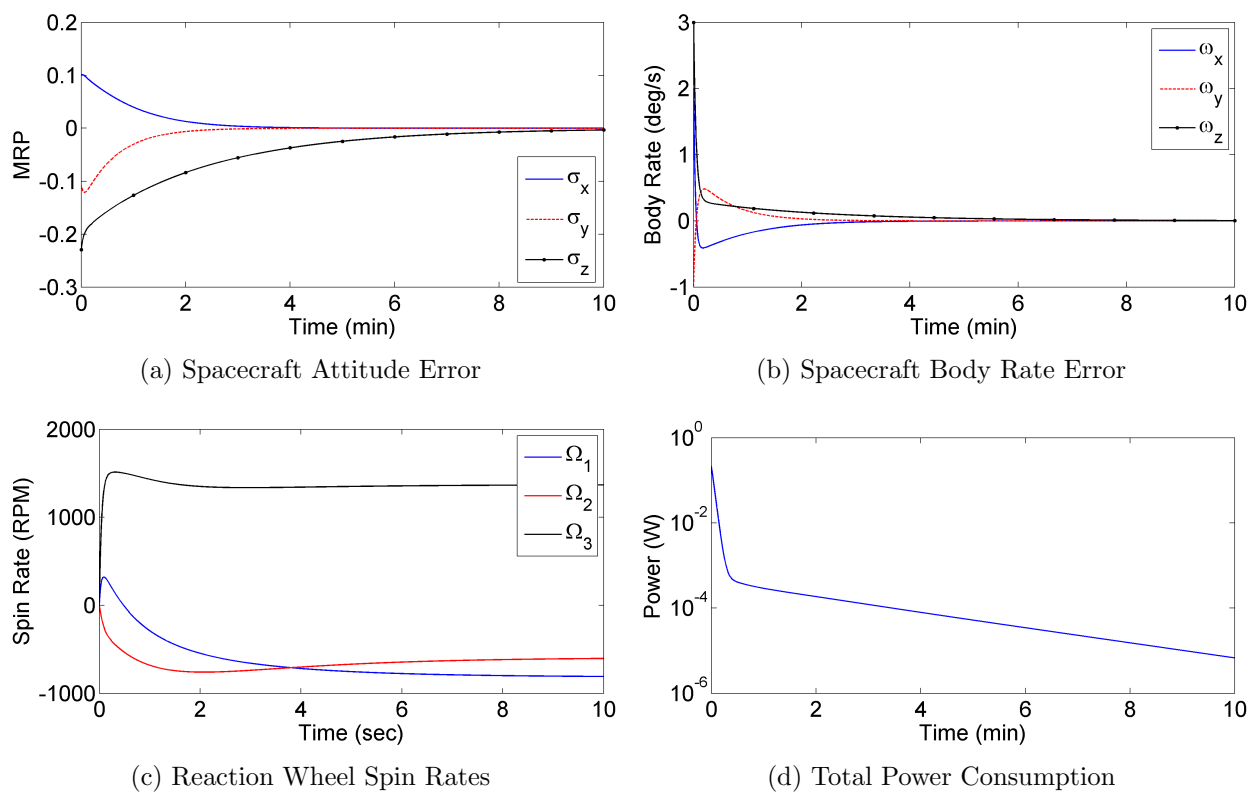


Figure 4.2: Reaction Wheel Cluster Attitude Control Maneuver

Chapter 5

Conclusions

A spherical actuator for spacecraft attitude control has been presented here that relies on a simple dipole magnet to exchange momentum with the spacecraft. The equations of motion for this system were derived and numerically simulated showing that the proposed actuator can indeed provide attitude control. A single spherical actuator was first examined and was able to successfully perform an attitude maneuver despite its inability to produce an arbitrary torque. Further research into this form of underactuated control will be necessary to fully understand how effective a single actuator can be. However, simulations conducted so far and analogous underactuated systems indicate that control arguments can be made.

A dual actuator configuration was also investigated and was found to successfully provide attitude control while at the same time requiring less power and energy than a single actuator. This could, however, be due to the fact that the dual actuator system simulated has twice the inertia of the single actuator system. A null motion control law was applied to the dual actuator system to avoid singularities and was able to rotate the rotors into a more favorable spin configuration without imparting a torque on the spacecraft. However, the effort needed to do this increased the total maneuver energy by a factor of five. More research into null motion control will be need to determine whether or not it's necessary or useful and how to implement it in an efficient manner.

Finally, the spherical actuator was compared against a cluster of three reaction wheels and was found to provide volume and power savings. The inertia about a spin axis was matched between the reaction wheel cluster and the spherical actuator as a basis for comparison. With this,

the spherical actuator was found to fill approximately half the volume of the reaction wheel cluster. On top of this, the peak power consumption of the spherical actuator was under a third of that for the reaction wheels, and the maneuver required less than half the total energy.

Although this thesis lays the groundwork for a spherical dipole actuator for attitude control and indicates this design is feasible and can provide potential volume and power savings, there are still many unanswered questions and many analyses that must be made to fully understand the capabilities and limitations of this device. Two possible issues that have not yet been investigated are induced magnetic dipole moments and system failure. In most spacecraft, shielding around the actuator is needed to prevent it from interfering with magnetometers, which provided guidance information and are used in many science applications. The problem with shielding the spherical actuator is the fact that magnetically permeable metals are needed, and as a result, their permeability would attract the rotor away from the center, in turn introducing a control disturbance and potentially destabilizing the system. In conventional motors, shielding is not as big of an issue because the rotor is mechanically held in place by bearings. A second potential issue with the spherical acuator also stems from the fact that the rotor is free-floating. If the ACS loses power and there is no backup system to maintain the position of the rotor, the rotor will impact the stator wall. If the rotor is spinning at high angular velocity, this would likely destroy the ACS and end the mission.

Aside from these problem areas, more research is needed to further this design. The next phase would likely include finite element modeling (FEM), rotor position and orientation sensing, and an experimental prototyping. FEM is needed because analytical force and torque solutions do not exist beyond the simplified model presented here. FEM would capture induced effects in the coils, eddy current loss in support structures and shielding, and an overall actuator model that's closer to reality. Sensing is another aspect that is not covered in this work, but is necessary for this device to function. Rotor position and orientation information is needed in the control laws and could likely be accomplished with hall effect sensors, though other sensing schemes have been examined [84–90]. In the end, an experimental model would be needed to validate this theoretical

work and bring this device closer to realization.

Whether or not the spherical dipole actuator will replace conventional attitude control systems is to be seen, however it could have a place in niche applications where active vibration damping and precision pointing are needed. Again, the results presented here show that the spherical dipole actuator has promise and is worth further investigation.

Bibliography

- [1] Schaub, H. and Junkins, J. L., Analytical Mechanics of Space Systems, AIAA Education Series, Reston, VA, 3rd ed., 2014.
- [2] Haeusseraiann, W., “Space vehicle attitude control mechanism,” Jan. 23 1962, US Patent 3,017,777.
- [3] Heinrich, C., Robert, C., Wilhelm, E., Aaron, G., and Fritz, K., “Spherical-flywheel attitude-control system,” Oct. 1 1963, US Patent 3,105,657.
- [4] Palm, W., System Dynamics, McGraw-Hill, Boston, Mass, 2010.
- [5] Tierney, T. E. and Curran, R. J., “Development of an electrostatic suspension reaction sphere,” New York, NY, United states, 1964.
- [6] Ormsby, R. and Smith, M., “Capabilities and limitations of reaction spheres for attitude control,” ARS Journal, Vol. 31, No. 6, 1961, pp. 808 – 812.
- [7] Isely, W., “Magnetically supported and torqued momentum reaction sphere,” Sept. 16 1986, US Patent 4,611,863.
- [8] Beams, J. and Young, J.L., I., “The production of high centrifugal fields,” Physical Review, Vol. 69, 1946/05/01, pp. 537 –.
- [9] Davey, K., Vachtsevanos, G., and Powers, R., “The analysis of fields and torques in spherical induction motors,” IEEE Transactions on Magnetics, Vol. MAG-23, No. 1, 1987/01, pp. 273 – 82.
- [10] Halverson, R. and Cohen, H., “Torque on a spinning hollow sphere in a uniform magnetic field,” IEEE Transactions on Aerospace, Navigation and Electronics, Vol. ANE-11, No. 2, 1964/06, pp. 118 – 122.
- [11] Hayes, A., “Torque on a spinning hollow sphere in a uniform alternating magnetic field,” IEEE Transactions on Aerospace, Navigation and Electronics, Vol. ANE-11, No. 2, 1964/06, pp. 122 – 127.
- [12] Hosny, W. and Dodds, S., “Analytical investigation of the torque capability of the reaction sphere,” Electric Machines and Power Systems, Vol. 25, No. 2, 1997/02, pp. 181 – 97.
- [13] Hosny, W. and Dodds, S., “Electromagnetic field analysis of the reaction sphere,” Aberdeen, UK, 1990, pp. 811 – 14.

- [14] Keith, J., “Magnetic torques and coriolis effects on a magnetically suspended rotating sphere,” Journal of Research of the National Bureau of Standards, Vol. 67D, No. 5, Sept. 1963, pp. 533 – 538.
- [15] Mrozynski, G. and Baum, E., “Analytical determination of eddy currents in a hollow sphere excited by an arbitrary dipole,” IEEE Transactions on Magnetics, Vol. 34, No. 6, 1998/11, pp. 3822 – 9.
- [16] Ruan, J., Huang, S., and Zhou, K., “Computation of 3D electromagnetic field and torques in spherical motors,” Vol. 17, UK, 1998, pp. 106 – 10.
- [17] Reichert, T., Nussbaumer, T., and Kolar, J., “Complete analytical solution of electromagnetic field problem of high-speed spinning ball,” Journal of Applied Physics, Vol. 112, No. 10, 2012/11/15, pp. 104901 (9 pp.) –.
- [18] Theodoulidis, T., Kantartzis, N., Tsiboukis, T., and Kriezis, E., “Analytical and numerical solution of the eddy-current problem in spherical coordinates based on the second-order vector potential formulation,” IEEE Transactions on Magnetics, Vol. 33, No. 4, 1997/07, pp. 2461 – 72.
- [19] Wildmann, C., Nussbaumer, T., and Kolar, J., “10 Mrpm spinning ball motor: preparing the next generation of ultra-high speed drive systems,” Piscataway, NJ, USA, 2010, pp. 278 – 83.
- [20] Wildmann, C., Nussbaumer, T., and Kolar, J., “Design considerations for the drive system of an ultra-high speed spinning ball motor,” Pisa, Italy, 2010, pp. 1478 – 1483.
- [21] Iwakura, A., “Feasibility Study on Three Dimensional Reaction Wheel,” Proceedings of the School of Science of Tokai University, Vol. 33, 2008, pp. 51–57.
- [22] Kumagai, M. and Hollis, R., “Development and control of a three DOF planar induction motor,” Piscataway, NJ, USA, 2012, pp. 3757 – 62.
- [23] Park, G., Yoon, H., Kim, D.-K., Yong, K.-L., and Petrov, S. E., “Feasibility study system conceptual design for the spherical actuator,” Gyeonggi-do, Korea, Republic of, 2011, pp. 1875 – 1879.
- [24] Shirasawa, Y. and Tsuda, Y., “Experimental study and analysis on three dimensional reaction wheel for microsatellites,” Vol. 130 PART 1, Galveston, TX, United states, 2008, pp. 507 – 517.
- [25] Williams, F., Laithwaite, E., and Eastham, J., “Development and design of spherical induction motors,” Proceedings of the Institution of Electrical Engineers. A. Power Engineering, Vol. 106, No. 30, 1959/12, pp. 471 – 483.
- [26] Dehez, B., Galary, G., Grenier, D., and Raucant, B., “Development of a spherical induction motor with two degrees of freedom,” IEEE Transactions on Magnetics, Vol. 42, No. 8, 2006/08, pp. 2077 – 89.
- [27] Vachtsevanos, G. J., Davey, K., and Lee, K.-M., “DEVELOPMENT OF A NOVEL INTELLIGENT ROBOTIC MANIPULATOR.” IEEE Control Systems Magazine, Vol. 7, No. 3, 1987, pp. 9 – 15.

- [28] Nakanishi, T., Ando, Y., Sakakibara, K., and Mitsukane, A., “Control moment gyro having spherical rotor with permanent magnets,” Dec. 19 1995, US Patent 5,476,018.
- [29] Chételat, O., “Torquer apparatus,” April 24 2012, US Patent 8,164,294.
- [30] Rossini, L., Onillon, E., Chételat, O., and Perriard, Y., “Back-EMF and rotor angular velocity estimation for a reaction sphere actuator,” Piscataway, NJ, USA, 2014, pp. 334 – 9.
- [31] Rossini, L., Onillon, E., Chételat, O., and Perriard, Y., “An optimal sensor placement strategy for force and torque analytical models of a reaction sphere actuator for satellite attitude control,” Piscataway, NJ, USA, 2012, pp. 2545 – 51.
- [32] Rossini, L., Chételat, O., Onillon, E., and Perriard, Y., “Analytical and experimental investigation on the force and torque of a reaction sphere for satellite attitude control,” Piscataway, NJ, USA, 2011, pp. 487 – 92.
- [33] Rossini, L., Chételat, O., Onillon, E., and Perriard, Y., “An open-loop control strategy of a reaction sphere for satellite attitude control,” Piscataway, NJ, USA, 2011, pp. 4 pp. –.
- [34] Rossini, L., Chételat, O., Onillon, E., and Perriard, Y., “Force and torque analytical models of a reaction sphere actuator based on spherical harmonic rotation and decomposition,” IEEE/ASME Transactions on Mechatronics, Vol. 18, No. 3, 2013/06, pp. 1006 – 18.
- [35] Rossini, L., Mingard, S., Boletis, A., Forzani, E., Onillon, E., and Perriard, Y., “Rotor Design Optimization for a Reaction Sphere Actuator,” IEEE Transactions on Industry Applications, Vol. 50, No. 3, 2014/05, pp. 1706 – 16.
- [36] Strumik, M., Wawrzaszek, R., Banaszkiwicz, M., Seweryn, K., Sidz, M., Onillon, E., and Rossini, L., “Analytical model of eddy currents in a reaction sphere actuator,” IEEE Transactions on Magnetics, Vol. 50, No. 6, 2014/06, pp. 4004607 (7 pp.) –.
- [37] Wawrzaszek, R., Strumik, M., Seweryn, K., Sidz, M., Banaszkiwicz, M., Rossini, L., and Onillon, E., “Electromagnetic compatibility problems of ELSA - Novel component for spacecraft attitude control system based on concept of spherical actuator,” Piscataway, NJ, USA, 2013, pp. 572 – 7.
- [38] Ackermann, B., Steinbusch, H., Vollmer, T., Wang, J., Jewell, G., and Howe, D., “A spherical permanent magnet actuator for a high-fidelity force-feedback joystick,” Mechatronics, Vol. 14, No. 3, 2004/04, pp. 327 – 39.
- [39] Bederson, B. B., Wallace, R. S., and Schwartz, E. L., “Miniature pan-tilt actuator: the spherical pointing motor,” IEEE Transactions on Robotics and Automation, Vol. 10, No. 3, 1994, pp. 298 – 308.
- [40] Ebihara, D., Katsuyama, N., and Kajioaka, M., “An approach to basic design of the PM-type spherical motor,” Vol. vol.2, Piscataway, NJ, USA, 2001, pp. 1792 – 7.
- [41] Gofuku, A., Sasaki, R., Yano, T., Wada, Y., and Shibata, M., “Development of a spherical stepping motor rotating around six axes,” International Journal of Applied Electromagnetics and Mechanics, Vol. 39, No. 1-4, 2012, pp. 905 – 11.

- [42] Kahlen, K., Voss, I., Priebe, C., and De Doncker, R., "Torque control of a spherical machine with variable pole pitch," IEEE Transactions on Power Electronics, Vol. 19, No. 6, 2004/11, pp. 1628 – 34.
- [43] Kaneko, K., Yamada, I., and Itao, K., "A spherical DC servo motor with three degrees of freedom," Transactions of the ASME. Journal of Dynamic Systems, Measurement and Control, Vol. 111, No. 3, Sept. 1989, pp. 398 – 402.
- [44] Lee, K.-M. and Kwan, C.-K., "Design concept development of a spherical stepper for robotic applications," IEEE Transactions on Robotics and Automation, Vol. 7, No. 1, 1991, pp. 175 – 181.
- [45] Lee, K.-M., Hungsun, S., and Joni, J., "Concept development and design of a spherical wheel motor (SWM)," Vol. 2005, Barcelona, Spain, 2005, pp. 3652 – 3657.
- [46] Lee, K.-M., Sosseh, R., and Wei, Z., "Effects of the torque model on the control of a VR spherical motor," Control Engineering Practice, Vol. 12, No. 11, 2004/11, pp. 1437 – 49.
- [47] Li, Z., "Intelligent control for permanent magnet spherical stepper motor," Qingdao, China, 2008, pp. 1807 – 1812.
- [48] Li, Z. and Wang, Q., "Robust neural network controller design for permanent magnet spherical stepper motor," Piscataway, NJ, USA, 2008, pp. 6 pp. –.
- [49] Lim, C. K., Chen, I.-M., Yan, L., Yang, G., and Lee, K.-M., "Electromechanical modeling of a permanent-magnet spherical actuator based on magnetic-dipole-moment principle," IEEE Transactions on Industrial Electronics, Vol. 56, No. 5, 2009, pp. 1640 – 1648.
- [50] Qian, Z., Wang, Q., Ju, L., Wang, A., and Liu, J., "Torque modeling and control algorithm of a permanent magnetic spherical motor," Tokyo, Japan, 2009, pp. IEEJ Industry Applications Society; The Korean Institute of Electrical Engineers (KIEE); China Electrotechnical Society (CES); Daikin Industries, Ltd.; Fuji Electric Systems Co., Ltd. –.
- [51] Rashid, M. and Khalil, Z., "Configuration design and intelligent stepping of a spherical motor in robotic joint," Journal of Intelligent and Robotic Systems: Theory and Applications, Vol. 40, No. 2, 2004/06, pp. 165 – 81.
- [52] Son, H. and Lee, K.-M., "Open-Loop Controller Design and Dynamic Characteristics of a Spherical Wheel Motor," IEEE Transactions on Industrial Electronics, Vol. 57, No. 10, 2010/10, pp. 3475 – 82.
- [53] Wang, J., Jewell, G., and Howe, D., "Analysis, design and control of a novel spherical permanent-magnet actuator," IEE Proceedings-Electric Power Applications, Vol. 145, No. 1, 1998/01, pp. 61 – 71.
- [54] Wang, W., Wang, J., Jewell, G., and Howe, D., "Design and control of a novel spherical permanent magnet actuator with three degrees of freedom," IEEE/ASME Transactions on Mechatronics, Vol. 8, No. 4, 2003/12, pp. 457 – 68.
- [55] Xia, C., Li, H., and Shi, T., "3-D magnetic field and torque analysis of a novel Halbach array permanent-magnet spherical motor," IEEE Transactions on Magnetics, Vol. 44, No. 8, 2008/08, pp. 2016 – 20.

- [56] Xia, C., Xin, J., Li, H., and Shi, T., “Design and Analysis of a Variable Arc Permanent Magnet Array for Spherical Motor,” IEEE Transactions on Magnetics, Vol. 49, No. 4, 2013/04, pp. 1470 – 8.
- [57] Xia, C., Song, P., Li, H., Li, B., and Shi, T., “Research on torque calculation method of permanent-magnet spherical motor based on the finite-element method,” IEEE Transactions on Magnetics, Vol. 45, No. 4, 2009/04, pp. 2015 – 22.
- [58] Yang, C. I. and Baek, Y. S., “Design and control of the 3 degrees of freedom actuator by controlling the electromagnetic force,” Vol. 35, USA, Sept. 1999, pp. 3607 – 9.
- [59] Yan, L., Chen, I.-M., Yang, G., and Lee, K.-M., “Analytical and experimental investigation on the magnetic field and torque of a permanent magnet spherical actuator,” IEEE/ASME Transactions on Mechatronics, Vol. 11, No. 4, 2006, pp. 409 – 418.
- [60] Yan, L., Chen, I.-M., Lim, C. K., Yang, G., Lin, W., and Lee, K.-M., “Design and analysis of a permanent magnet spherical actuator,” Edmonton, AB, Canada, 2005, pp. 2607 – 2612.
- [61] Yan, L., Chen, I.-M., Lim, C. K., Yang, G., Lin, W., and Lee, K.-M., “Hybrid torque modeling of spherical actuators with cylindrical-shaped magnet poles,” Mechatronics, Vol. 21, No. 1, 2011/02, pp. 85 – 91.
- [62] Yan, L., Chen, I.-M., Lim, C. K., Yang, G., and Lee, K.-M., “Modeling and Iron-Effect Analysis on Magnetic Field and Torque Output of Electromagnetic Spherical Actuators With Iron Stator,” IEEE/ASME Transactions on Mechatronics, Vol. 17, No. 6, 2012/12, pp. 1080 – 7.
- [63] Yano, T., “Proposal of polyhedron based spherical stepping motors,” Piscataway, NJ, USA, 2008/06/11, pp. 1433 – 8.
- [64] Zhou, Z. and Lee, K.-M., “Real-time motion control of a multi-degree-of-freedom variable reluctance spherical motor,” Vol. vol.3, New York, NY, USA, 1996, pp. 2859 – 64.
- [65] Zhu, Z., Howe, D., and Chan, C., “Improved analytical model for predicting the magnetic field distribution in brushless permanent-magnet machines,” IEEE Transactions on Magnetics, Vol. 38, No. 1, 2002/01, pp. 229 – 38.
- [66] Zhu, Z., Howe, D., Bolte, E., and Ackermann, B., “Instantaneous magnetic field distribution in brushless permanent magnet DC motors. I. Open-circuit field,” IEEE Transactions on Magnetics, Vol. 29, No. 1, 1993/01, pp. 124 – 35.
- [67] Zhu, Z. and Howe, D., “Instantaneous magnetic field distribution in brushless permanent magnet DC motors. II. Armature-reaction field,” IEEE Transactions on Magnetics, Vol. 29, No. 1, 1993/01, pp. 136 – 42.
- [68] Zhu, Z. and Howe, D., “Instantaneous magnetic field distribution in brushless permanent magnet DC motors. III. Effect of stator slotting,” IEEE Transactions on Magnetics, Vol. 29, No. 1, 1993/01, pp. 143 – 51.
- [69] Yan, L., Chen, I.-M., Son, H., Lim, C. K., and Yang, G., “Analysis of Pole Configurations of Permanent-Magnet Spherical Actuators,” IEEE/ASME Transactions on Mechatronics, Vol. 15, No. 6, 2010/12, pp. 986 – 9.

- [70] Jinjun, G., Kim, D.-H., and Son, H., “Effects of Magnetic Pole Design on Orientation Torque for a Spherical Motor,” IEEE/ASME Transactions on Mechatronics, Vol. 18, No. 4, 2013/08, pp. 1420 – 5.
- [71] Yan, L., Chen, I.-M., Lim, C. K., Yang, G., Lee, K.-M., and Lin, W., “Empirical formulation of torque output for spherical actuators with low-cost rotor poles,” Singapore, Singapore, 2009, pp. 1625 – 1630.
- [72] Chirikjian, G. and Stein, D., “Kinematic design and commutation of a spherical stepper motor,” IEEE/ASME Transactions on Mechatronics, Vol. 4, No. 4, 1999/12, pp. 342 – 53.
- [73] Lee, K.-M., Bai, K., and Lim, J., “Dipole models for forward/inverse torque computation of a spherical motor,” IEEE/ASME Transactions on Mechatronics, Vol. 14, No. 1, 2009/02, pp. 46 – 54.
- [74] Lee, K.-M. and Son, H., “Distributed multipole model for design of permanent-magnet-based actuators,” IEEE Transactions on Magnetics, Vol. 43, No. 10, 2007, pp. 3904 – 3913.
- [75] Tsiotras, P., “A Passivity Approach to Attitude Stabilization Using Nonredundant Kinematic Parameterizations,” Proceedings of the 34th IEEE Conference on Decision and Control, Vol. 1, 1995, pp. 515–20.
- [76] Lovera, M., De Marchi, E., and Bittanti, S., “Periodic attitude control techniques for small satellites with magnetic actuators,” IEEE Transactions on Control Systems Technology, Vol. 10, No. 1, 2002/01, pp. 90 – 5.
- [77] Psiaki, M., “Magnetic torquer attitude control via asymptotic periodic linear quadratic regulation,” Journal of Guidance, Control, and Dynamics, Vol. 24, No. 2, 2001/03, pp. 386 – 94.
- [78] Wisniewski, R., “Linear time-varying approach to satellite attitude control using only electromagnetic actuation,” Journal of Guidance, Control, and Dynamics, Vol. 23, No. 4, 2000/07, pp. 640 – 7.
- [79] Silani, E. and Lovera, M., “Magnetic spacecraft attitude control: a survey and some new results,” Control Engineering Practice, Vol. 13, No. 3, 2005/03, pp. 357 – 71.
- [80] Astolfi, A. and Lovera, M., “Global spacecraft attitude control using magnetic actuators,” Vol. vol.2, Danvers, MA, USA, 2002, pp. 1331 – 5.
- [81] Pittelkau, M., “Optimal periodic control for spacecraft pointing and attitude determination,” Journal of Guidance, Control, and Dynamics, Vol. 16, No. 6, 1993/11, pp. 1078 – 84.
- [82] Bhat, S., “Controllability of nonlinear time-varying systems: applications to spacecraft attitude control using magnetic actuation,” IEEE Transactions on Automatic Control, Vol. 50, No. 11, 2005/11, pp. 1725 – 35.
- [83] Technologies, B. C., “Micro Reaction Wheel,” 2015.
- [84] Chen, W., Zhang, L., Yan, L., and Liu, J., “Design and control of a three degree-of-freedom permanent magnet spherical actuator,” Sensors and Actuators A (Physical), Vol. 180, 2012/06, pp. 75 – 86.

- [85] Fang, W. and Son, H., “Optimization of Measuring Magnetic Fields for Position and Orientation Tracking,” IEEE/ASME Transactions on Mechatronics, Vol. 16, No. 3, 2011/06, pp. 440 – 8.
- [86] Hu, L., Lee, K.-M., and Fu, X., “A method based on measured boundary conditions for reconstructing the magnetic field distribution of an electromagnetic mechatronic system,” IEEE/ASME Transactions on Mechatronics, Vol. 15, No. 4, 2010, pp. 595 – 602.
- [87] Hu, Y., Chen, J., and Ding, X., “Analysis and Computation on Magnetic Field of Solid Rotor Induction Motor,” IEEE Transactions on Applied Superconductivity, Vol. 20, No. 3, 2010/06/, pp. 1844 – 7.
- [88] Foong, S., Lee, K.-M., and Bai, K., “Magnetic field-based sensing method for spherical joint,” Piscataway, NJ, USA, 2010, pp. 5447 – 52.
- [89] Stein, D., Scheinerman, E., and Chirikjian, G., “Mathematical models of binary spherical-motion encoders,” IEEE/ASME Transactions on Mechatronics, Vol. 8, No. 2, 2003/06, pp. 234 – 44.
- [90] Yan, L., Chen, I.-M., Guo, Z., Lang, Y., and Li, Y., “A three degree-of-freedom optical orientation measurement method for spherical actuator applications,” IEEE Transactions on Automation Science and Engineering, Vol. 8, No. 2, 2011/04, pp. 319 – 26.

Appendix A

Algebraic Force and Torque Expressions

If the rotor is centered in the stator, explicit expressions for \mathbf{F}_k and \mathbf{T}_k exist and are given by

$$\mathbf{F}_k = \frac{i_k N}{A} \begin{pmatrix} \frac{\mu_0 \|\mathbf{m}\| (\ln(R_a) - \ln(R_b)) (\sin(\theta_a)^3 - \sin(\theta_b)^3) (C_{31} \cos(\beta) \sin(\alpha) - C_{33} \cos(\alpha) + C_{32} \sin(\alpha) \sin(\beta))}{4} \\ \frac{\mu_0 \|\mathbf{m}\| (\ln(R_a) - \ln(R_b)) (\sin(\theta_a)^3 - \sin(\theta_b)^3) (C_{32} \cos(\beta) - C_{31} \sin(\beta))}{4} \\ - \frac{\mu_0 \|\mathbf{m}\| (\ln(R_a) - \ln(R_b)) (\sin(\theta_a)^3 - \sin(\theta_b)^3) (C_{33} \sin(\alpha) + C_{31} \cos(\alpha) \cos(\beta) + C_{32} \cos(\alpha) \sin(\beta))}{2} \end{pmatrix}$$

$$\mathbf{T}_k = \frac{i_k N}{A} \begin{pmatrix} - \frac{\mu_0 \|\mathbf{m}\| (R_a - R_b) (2\theta_a - 2\theta_b - \sin(2\theta_a) + \sin(2\theta_b)) (C_{32} \cos(\beta) - C_{31} \sin(\beta))}{8} \\ \frac{\mu_0 \|\mathbf{m}\| (R_a - R_b) (2\theta_a - 2\theta_b - \sin(2\theta_a) + \sin(2\theta_b)) (C_{31} \cos(\beta) \sin(\alpha) - C_{33} \cos(\alpha) + C_{32} \sin(\alpha) \sin(\beta))}{8} \\ 0 \end{pmatrix}$$

where α and β are the latitude and longitude of the coil of interest with respect to the spacecraft body frame.